

Electrochemical Properties and Theoretical Capacity for Sodium Storage in Hard Carbon: Insights from First Principles Calculations

Clement Bommier,^{†,§,||} Xiulei Ji,[†] and P. Alex Greaney^{*‡,§,||}

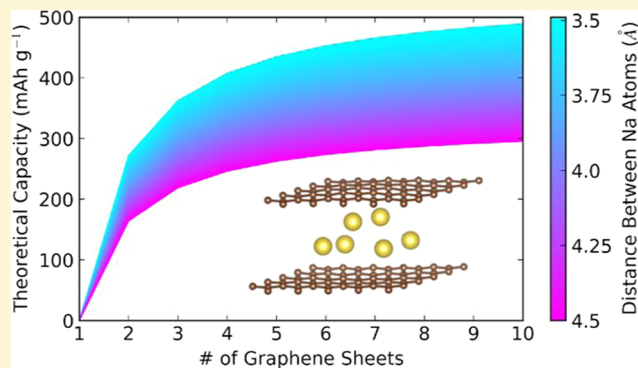
[†]Department of Chemistry, Oregon State University, Corvallis, Oregon 97331, United States

[‡]Materials Science and Engineering, University of California—Riverside, Riverside, California 92507, United States

[§]Department of Mechanical and Aerospace Engineering and ^{||}Andlinger Center for Energy and the Environment, Princeton University, Princeton, New Jersey 08540, United States

Supporting Information

ABSTRACT: This paper utilizes density functional theory calculations to explore amorphous carbon materials, and concludes that the theoretical capacity is between 300 and 400 mAh g⁻¹, depending on the degree of defects. This conclusion arises from a comprehensive number of simulations used to validate the experimentally determined storage mechanism, with these results then being extrapolated to elucidate a theoretical capacity limit. Through investigating the breadth of structures, with multiple Na configurations, the studies lead to four major conclusions. First, we found that the nature of Na storage in carbon materials changes with increasing Na concentrations in a continuum from ionic storage to metallic plating. Second, we revealed the critical role of the intersheet spacing, stacking misalignment, and effects of spacing expansion on the feasibility of Na intercalation into graphitic structures. This leads to the third and fourth conclusion, which stipulates that the results provided here offer compelling support towards an earlier experimentally derived Na ion storage for hard carbon materials, along with the existence of a theoretical limit of sodium ion storage in hard carbon materials. Moreover, the techniques and scope of the work involved are highly relevant to future simulations exploring amorphous carbon as an active material, whether it should be for Li-ion battery anodes, supercapacitors, or catalysts.



1. INTRODUCTION

Success at meeting the 2 °C warming limit set forth at the 2015 Paris climate agreement is contingent on superseding CO₂ generating power sources with renewable energy systems. However, switching to renewable energy faces a central constraint, that is, due to its intermittency, such sources with energy storage solutions are unfeasible. Moreover, Li-ion batteries (LIBs), the current state-of-the-art commercially available batteries, although ideally suited for this task in principle, face issues of cost and scalability, thus greatly curtailing their potential as grid-level energy storage solutions.¹ However, relatively newer technologies, such as Na-ion batteries (NIBs), present themselves as a promising alternative.²

NIBs have many electrochemical similarities to LIBs, but offer greater potential scalability, due to lesser reliance on raw materials such as cobalt and lithium for the cathode.^{3–5} However, the state of the anode remains a major impediment to their commercialization. Although LIBs can make use of a graphitic anode, forming a reversible LiC₆ graphite intercalation compound (GIC) in the charged state, sodium atoms can only manage a NaC₆₄ GIC, making graphite an ill-suited NIB anode.^{6,7} This reluctance to intercalate comes from

unfavorable thermodynamics involving the ionic size and electron transfer potential.^{8–10} This issue has motivated a hunt for alternate materials, and among those studied, various forms of amorphous, graphite-like carbon are considered most promising.^{11–14} The expanded and more defective nature of these materials loosens the size and energetic constraints of crystalline graphite, allowing for reversible sodium atom storage^{15,16} with capacities reported in the 300–350 mAh g⁻¹ range—which are in the range of the 372 mAh g⁻¹ theoretical capacity of LiC₆.^{17–19} Additionally, these carbons also have a wide variety of complex morphologies, controllable porosity, and ability to be doped with heteroatoms, thus rendering them extremely useful for tailor made battery applications.^{20,21}

A majority of the amorphous carbons used for NIB anodes can be classified under the hard carbon variety.^{12,22,23} The other variety is soft carbon, but the structure and electrochemical properties are slightly different and will not be covered in this paper.^{24,25} The structure of hard carbons can be

Received: April 4, 2018

Revised: December 15, 2018

Published: December 17, 2018

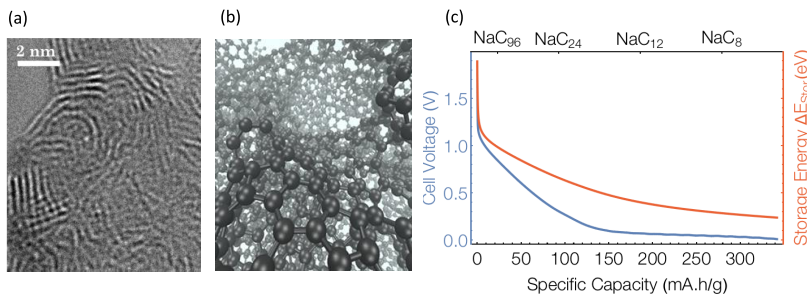


Figure 1. (a) Transmission electron microscopy image of a hard carbon anode showing the misaligned, curved, and disordered graphene stacks. (b) Schematic from a molecular dynamics simulation of a theoretical amorphous carbon system, showing the extent of the structural disorder. (c) A typical sodiation profile of a hard carbon/Na half-cell during its third discharge cycle. The blue line shows the experimentally measured cell voltage relative to the Na metal. The red line shows the corresponding mean storage energy per energy sodium atom—the quantity computed from total energy calculations. The relationship between the blue and red curves is described in eq 5. Recent models of sodium storage attribute the sloping portion of the sodiation profile to storage as defect sites and the long plateau region to intercalation into the galleries of graphitic nanodomains. The very end of the low voltage plateau is thought to mark the onset of plating.

described briefly as a patchwork of rumpled and twisted graphene nanodomains trapping pockets of empty pore space (Figure 1a,b). In the nanodomains, the stacked sheets are disordered along the c-axis. Furthermore, the structure possesses a number of defective sites, such as monovacancies, divacancies, edge carbons, and dangling bonds. The concentration of these defect sites varies from sample to sample, and can best be established via pair-distribution function measurements or Raman scattering.^{26–28} This internal structure varies with precursors and synthesis conditions and gives rise to a bewildering array of amorphous carbons, with different sodium storage properties.

The different structural features are manifested experimentally in galvanostatic charge/discharge curves of amorphous carbons, which differ in shape and capacity. Figure 1c shows a typical sodiation profile for a hard carbon synthesized from the pyrolysis of sucrose at 1400 °C.²⁹ To date, much research has been devoted to elucidating the mechanisms of sodium storage, and in particular to tie features in the sodiation potential profile to aspects of the structure, with the hope of uncovering morphologies needed to achieve optimal electrochemical performances. These models, starting in the early 2000's by Dahn et al.,¹⁶ to later models in the early to mid 2010's by Mitlin et al.,¹⁷ Ji et al.,²⁹ Tarascon et al.,³⁰ and Grey et al.,³¹ all aim to provide sodium storage mechanisms—though they stop short of outlining a theoretical limit to sodium atom storage.

These are divided into two categories. The first one is similar to the Dahn's model. It proposes that sodium storage occurs first via intercalation into the galleries of graphitic domains, followed by storage of sodium ions in pores near the low voltage plating potential. The other models, despite small variations, all propose that storage occurs first at defective sites on the carbon structure, then with a combination of intercalation into graphene nanodomains, and in micropores, with the intercalation and micropore storage occurring in the low voltage plateau region of hard carbon.

The work presented in this article scrutinizes the hypothesized storage mechanisms by density functional theory (DFT) calculations of energy and electronic structure of Na/C interactions. In doing so, the work also takes on a larger goal, that is, to establish what theoretical limits exist for hard carbon's capacity to store sodium. This step is vital for further NIB progress, as it will outline how much room for

improvement exists with regard to capacity in hard carbon anodes for NIBs.

The simulations using an assortment of different carbon substrates and Na configurations. These reveal the electronic structure of the bonding interaction and enable us to disentangle assorted structural contributions to the interaction energy. From these calculations one can infer the sodiation mechanisms of amorphous carbon and identify structural contributions to the total storage capacity. The calculations do not exactly replicate real anode materials, but they provide insightful parallels that can be applied to the models describing the experimental results.

What sets this work apart from computational studies that have preceded this^{9,32–42} is the extent to which we have surveyed different Na/C systems. The results lead us to four major conclusions that are only evident because of the breadth of structures studied. Specifically, (1) we find that the nature of Na storage in carbon materials changes with increasing Na concentrations in a continuum from ionic storage to metallic plating; (2) we reveal the critical role of the intersheet spacing, stacking misalignment, and effects of spacing expansion with regard to intercalation; (3) the results provide compelling support towards an earlier experimentally derived Na ion storage for hard carbon materials; and (4) the elucidation of a theoretical limit of sodium ion storage in hard carbon materials. Additionally, the insights gained into the electrochemical behavior of hard carbon, such as the high-energy binding at defect sites, buckling nature of intercalated graphene domains, or attempts to pin down theoretical capacity limits have implications in other fields utilizing hard carbon, such as LIB anodes, supercapacitors, and catalysts—thus transcending the original NIB-centric research.

2. COMPUTATIONAL APPROACH

In the present work, our utilization of DFT calculations revolves around a simple premise, that is, is the energy change between the final Na/C configuration and the Na and C, as individual components, enough to overcome the energy of removing a Na atom from a bulk body-centered cubic (BCC) configured metal host? We refer to this change in energy for moving a Na atom from Na metal to some storage environment in the carbon anode as the storage energy. Rather than simply computing the storage energy for different idealized anode configurations, we also compute the energy hypothetical insertion path of a sodium atom so as to tease

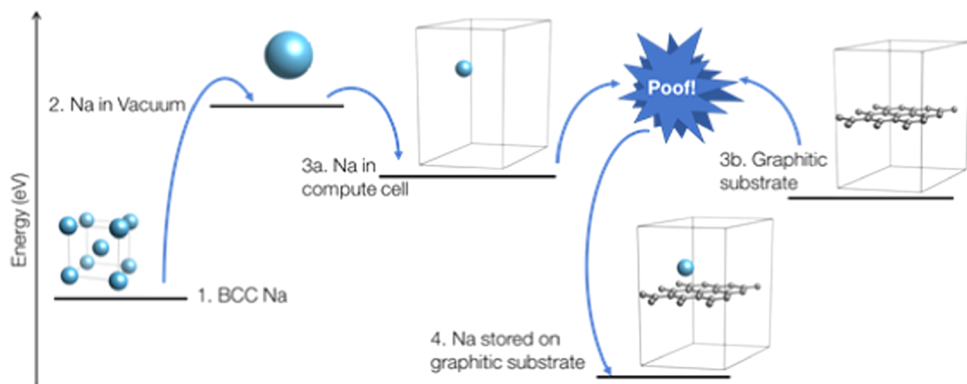


Figure 2. Hypothetical energy path for the storage of Na by removing a single Na atom from the metal crystal and combining it with a bare graphene sheet to form the final Na/C configuration.

apart the contribution to the storage energy from several contributing factors. This concept is illustrated in Figure 2, which shows the overall energy path of the Na atom and carbon structure from their original configurations into the final state.

2.1. Computed Parameters. For the calculations, we used a total of four different energies, from which all subsequent values are derived. The first parameter is that of Na in a BCC cell (Figure 2.1), which was determined to be -1.31 eV per Na atom. The second parameter is Na in a computed cell (Figure 2.3a), as well as a graphitic substrate in the same computed cell (Figure 2.3b). There was no need to consider the intermediary of Na going to a vacuum state, as the process of moving a sodium atom from a BCC unit cell to a computed cell is a state function, thus rendering it path independent. The last parameter is the simulation of the Na atom or Na atoms with a graphitic substrate (Figure 2.4). The computed cell used in Figure 2.3a, 3b, 4 is of identical size, so periodic boundary conditions are the same in all three cases. Furthermore, all the values obtained in the four parameters represent equilibrium positions. We never computed specific points along the path to Na storage, and since the energies are representative of equilibrium states, we do not need to calculate energies at intermediate steps, as the equilibrium energy is path independent.

Different concentrations of Na were simulated by shrinking or expanding the carbon substrate, thus changing the C to Na ratio. Although this is an effective way of simulating different states of charge, it imposes that the Na atoms are equivalently spaced due to the periodic boundary conditions in the DFT model. We realize that this is not necessarily physical, and thus we conducted additional simulations with multiple Na atoms in the same cell so as to study Na–Na interactions unrestricted by periodicity (these are described later in the article). Furthermore, we must emphasize that these idealized carbon substrates with their uniformly spaced Na atoms are not intended to perfectly mimic what is occurring in an actual hard carbon structure; however, these simulations are meant to be representative of the Na storage process in hard carbon, revealing trends in sodiation and enabling us to estimate a theoretical limit of capacity.

The storage energy, $\Delta E_{\text{storage}}(\chi)$, is the energy per atom to store Na atoms at a concentration χ Na atoms per C atom in the substrate. This is the same energy that would be found in a C/Na half-cell where overpotentials, entropy, and extraneous effects from electrolyte, solid electrolyte interphase (SEI), and

separators are not considered. As such, $\Delta E_{\text{storage}}$ is related to each other. In a calculation of x Na atoms stored on a substrate of N C atoms this is given by

$$\Delta E_{\text{storage}} = \frac{E_{\text{Na}_x + \text{C}_N} - (xE_{\text{Na}_{\text{BCC}}} + E_{\text{C}_N})}{x} \quad (1)$$

where $E_{\text{Na}_x + \text{C}_N}$ is the total energy of the combined sodium graphene system, E_{C_N} is the energy of the N atom substrate by itself, and $E_{\text{Na}_{\text{BCC}}}$ is the cohesive energy per atom of Na metal. The sodium concentration or stored capacity is $\chi = x/N$, which gives a storage stoichiometry of $\text{NaC}_{1/\chi}$. Looking at the path in Figure 2, we can imagine decomposing the storage energy into two contributions, a contribution from the Na–Na interactions, and a contribution from Na/C interactions.

$$\Delta E_{\text{storage}} = \Delta E_{\text{Na–Na}}(\chi) + \Delta E_{\text{Na/C}}(\chi) \quad (2)$$

The energy $\Delta E_{\text{Na–Na}}(\chi)$ is the energy to bring a sodium atom from the BCC metal into the DFT computational simulation before the graphene substrate is added, and is given by

$$\Delta E_{\text{Na–Na}}(\chi) = \frac{E_{\text{Na}_x \text{ cell}} - xE_{\text{Na}_{\text{BCC}}}}{x} \quad (3)$$

In the cell used for computation, the Na interacts with its images across the cell's periodic boundaries, and so the system energy $E_{\text{Na}_x \text{ cell}}$ includes some contribution from Na–Na interactions that vary with the dimensions of the cell.

The $\Delta E_{\text{Na/C}}$ term represents the interaction between the sodium atom and the carbon substrate, whereas discounting the Na–Na interactions that occur in the unit cell, essentially resulting in ionic interactions between the Na and the carbon. This equation can also be written as

$$\Delta E_{\text{Na/C}} = \frac{E_{\text{Na}_x + \text{C}_N} - (E_{\text{Na}_x \text{ cell}} + E_{\text{C}_N})}{x} \quad (4)$$

The voltage, $V(\chi)$ measured in the discharge profile in Figure 1c is the electrochemical potential for Na insertion, that is, the energy required to add or remove an extra electron. This is related to the storage energy computed through DFT by the integral

$$\Delta E_{\text{storage}}(\chi) = \frac{1}{e} \int_0^x eV(\chi') d\chi' \quad (5)$$

where e is the charge of an electron. In Figure 1c, the integral in eq 5 used to compare the storage energy, which can also be

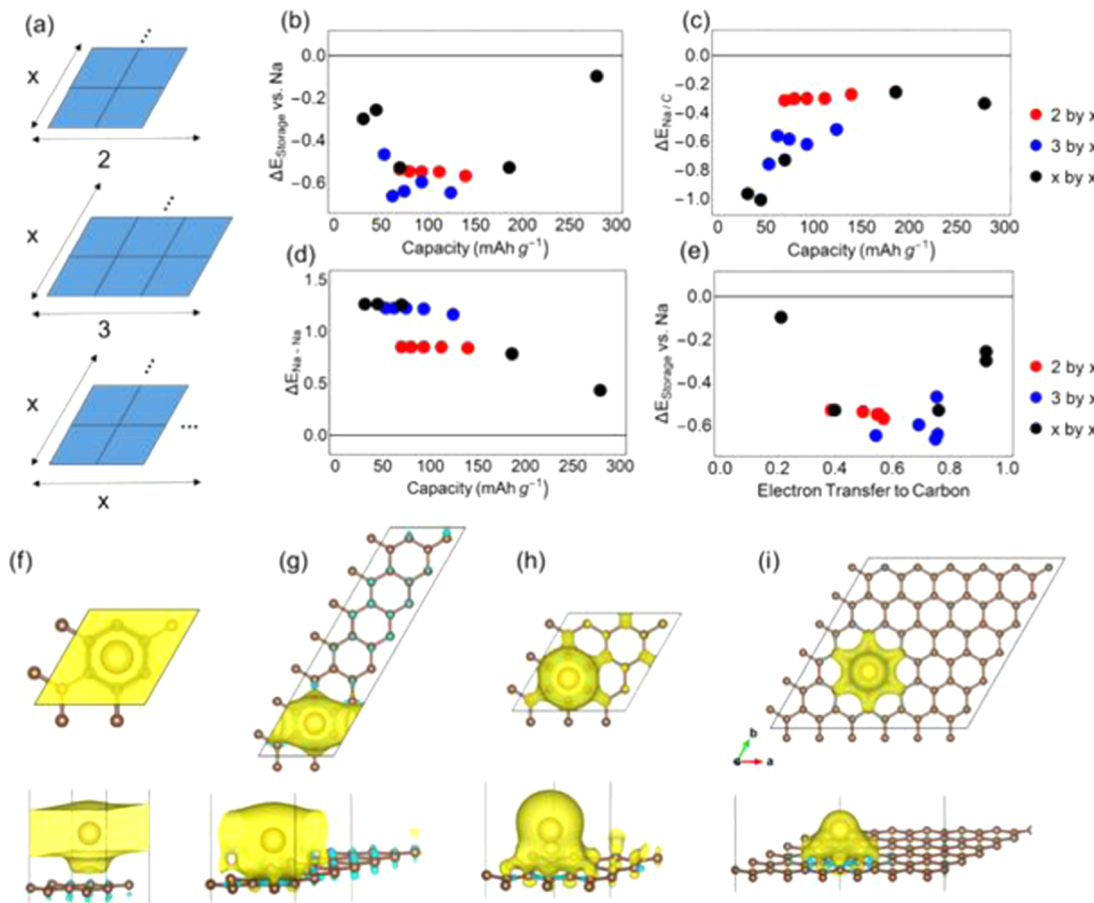


Figure 3. (a) Schematic for the different types of graphene geometries. (b) Measured $\Delta E_{\text{storage}}$ vs Na metal using eq 1. (c) $\Delta E_{\text{Gr-Na}}$, measuring the interaction between the sodium atom and the graphene sheet, whereas excluding contributions from the Na–Na interactions, as shown in eq 3. (d) $\Delta E_{\text{Na-Na}}$, measuring the Na–Na metallic interactions specific to the unit cell geometry. (e) $\Delta E_{\text{storage}}$ vs electron transfer. Charge distribution maps of (f) 2×2 , (g) 2×7 , (h) 3×3 , and (i) 6×6 graphene cell sizes following ionic relaxation. All isosurface values are of the same scale. Yellow isosurfaces represent regions electron density loss, whereas azure isosurfaces represent regions of electron density gains.

looked at as theoretical Na/C half-cell potential, is plotted in red for the experimentally measured sodiation potential of hard carbon plotted in blue. This creates some difficulty for direct comparison of DFT computed storage energies and experimentally measured storage potential. The sodiation process in hard carbon that yields the discharge potential shown in Figure 1c includes sodium storage on many different kinds of storage sites and the contribution from all of them is subsumed into the same integration. An alternative is to compare this differential form of this relationship which just uses the potential at a given storage concentration.

$$\Delta E_{\text{storage}}(\chi) + \chi \frac{d\Delta E_{\text{storage}}(\chi)}{d\chi} = eV(\chi) \quad (6)$$

This expression relates the storage energy to voltage at a single point in the sodiation cycle, and thus, if one assumes that different classes of sodium storage sites (e.g., storage at defects or interpolation into galleries) operate sequentially, then one can attribute the voltage to a bonding site. However, it is still not easy to equate this to a computed storage energy without knowing the fraction of the overall storage concentration χ that is associated with the particular storage environment. Moreover, as will be seen below, it is difficult to accurately compute the derivative of the storage energy with respect to concentration. In view of these problems, we do not use any

single calculation to infer the nature of sodium storage in amorphous carbon. Instead, we make an extensive survey of Na interacting with many different idealized substrates computing the energy and electronic structure in each case. From this combined data, we use trends in behavior on idealized substrates to infer the mechanism of storage in more messy real anode materials, and use quantitative values of storage energy only as a guide to set the magnitude of storage rather than direct comparison to points on the galvanostatic discharge curve. Furthermore, though the scope of this paper centers around Na, these first-principle assumptions would hold true for all other electrochemical systems.

The sets of calculations are divided into four groups, that is, Na on pristine graphene, Na on defective graphene, Na between bilayer graphene, and multiple Na atoms forming embryonic clustering on graphene. These suites of calculations reveal the role of Na concentration and Na–Na interactions, the relative effectiveness of defects as storage sites, the penalties associated with prying open graphite galleries to insert Na, and the propensity for clustering and the onset of plating.

2.2. Computational Details. Calculations were performed with the Vienna ab initio simulation package^{43–45} using projector augmented wave pseudopotentials^{46,47} with the generalized gradient approximation and the Perdew–Burke–Ernzerhof exchange–correlation functional.⁴⁸ The DFT-D3

method was used so as to accurately account for the long-range van der Waals forces present within the system.^{49,50} Wave functions were represented with a sum of plane waves up to an energy cut-offs of 500 eV, and a $6 \times 6 \times 1$ Monkhorst–Pack k -point sampling scheme was used for the Brillouin zone integration of the monolayer graphene sheets, whereas a $4 \times 4 \times 2$ scheme was used for the bilayers.⁵¹ The Na electronic structure was modeled including semicore electrons.

A variety of model graphene-based substrate materials were generated and ionically relaxed until the force present was of less than 0.01 eV Å⁻¹. Various graphene substrates were designed using a Matlab script, which effectively tiled a graphene unit cell to achieve the desired configuration—the script is available upon request to the corresponding author.

For the graphene unit cell, the original bond length was set to 1.41 Å, with the graphene substrate being placed in a supercell with 10 Å of vacuum on both sides of the substrate. The 10 Å vacuum space was determined by conducting a series of simulations where a sodium atom was gradually raised above the graphene to see the extent of interaction. The interactions mostly fade around 10 Å, as the energy of the system plateaus out (Figure S1). A 3×3 graphene substrate was used for the validation of parameters, and when ionically relaxed until present forces were less than 0.01 eV Å⁻¹, the unit cell changed from a volume of 929–958 Å³ (Table S1), which amounts to an increase of 3%. The average bond length between the carbon atoms of 1.425 Å is close to the experimental values, and has been reported by others.³⁷ The average energy per individual carbon atom under these parameters was computed to be -9.31 eV per atom.

The use of the DFT-D3 method, long-range van der Waals interactions, was also validated through the calculation of a 4×4 AB bilayer, which was computed both with and without van der Waals interactions. Using the DFT-D3 interactions, and a $4 \times 4 \times 2$ k -point scheme, the average d -spacing was found to be 3.41 Å, whereas the d -spacing without the DFT-D3 interactions was found to be 4.01 Å. The actual d -spacing measured through diffraction is of 3.35 Å, thus justifying the use of the DFT-D3 method (Figure S2).

The energy of Na storage on these substrates was obtained by comparing the value of the final structure with the sodium atom to that of the unsodiated graphene structure and the energy of a sodium metal atom in a BCC unit cell, which was found to be -1.31 eV and in good agreement with prior studies.³²

3. RESULTS

3.1. Storage of Na on Graphene. The first set of simulations explores the interaction between a sodium atom and a pristine graphene sheet. In this task, the NaC_x concentration is tuned by changing the size of the graphene patch, and as such, the size of the unit cell. To decouple the C_x to Na ratios from the Na–Na interactions, we provide three different geometries to vary the cell size of the substrate, using a graphene unit cell as a basis. As such, the substrate geometries are $2 \times x$, $3 \times x$, and $x \times x$, as demonstrated in the schematic in Figure 3a. Such a method allowed us to probe the dependency, if any, of the Na atom interactions with graphene sheets based on the cell geometry.

From the initial results seen in Figure 3b, we can see that Na interacting with the graphene substrate cannot overcome the energy of the Na_{BCC} metal. At low concentrations of Na, the storage energy is close to -0.25 eV. As the concentration

increases, the voltage decreases, with values close to -0.6 eV at its lowest point. However, after the concentration reaches a critical point, the storage energy begins to increase again. This is most evident with the voltage obtained from the 2×2 unit cell, an equivalent sodiation of NaC₈. At such a concentration, the storage energy is close to -0.1 eV. This is considerably higher than what it was at extremely lower NaC_x ratios, which suggests a changing storage mechanism as the concentration increases.

Although the storage energy versus capacity chart shows little dependence on cell morphology, this narrative changes when factoring the Na–Na interactions from the unit cell. As seen in Figure 3c, the trend between storage energy and capacity is affected by two factors: Na concentration and cell geometry. The former is expected. As the concentration of Na on the substrate increases, the ionic interactions are attenuated, as the concentration of electrons to be stored per unit area is larger.

However, we also see that $\Delta E_{\text{Na–Na}}$ and $\Delta E_{\text{Na/C}}$ is strongly dependent on the geometry. Although some of the $2 \times x$, $3 \times x$, and $x \times x$ —ranging from 2×2 to 6×6 —substrates have the same concentration, they have very different $\Delta E_{\text{Na–Na}}$ and $\Delta E_{\text{Na/C}}$ which are governed by cell morphology. This must be due to the Na–Na metal interactions across the periodic boundary conditions. Such interactions are stronger in a $2 \times x$ cell than they would be in a $3 \times x$ or $x \times x$ cell, as the distance between Na atoms is reduced in the lateral direction at Figure 3d, as well as the electron density gain/loss plots in Figure 3f–i. In the electron density gain/loss plots, we see that for the 2×2 and $2 \times x$ unit cells, the region of electron density loss is spread out over neighboring sodium atoms, thus attesting to the Na–Na interactions. However, in the larger unit cells, the electron density loss is confined to a single sodium atom, thus making its interaction with the carbon substrate more ionic. Yellow isosurfaces represent regions of electron density loss that occur when electrons from the Na interact with the graphene. Conversely, the azure isosurfaces represent regions of electron density gain.

As we can see in the charge distribution plots, the Na atom in the 2×2 and the 2×7 cell shares its charge with the neighboring unit cell. This occurs to a slightly lesser extent in the 3×3 cell, and does not occur at all in the 6×6 cell.

This preference between the sharing of charge between Na atoms due to proximity, as opposed to the transfer of the charge to the graphene sheet, gives us a good insight into the charging storage mechanism as a function of Na concentration on the graphene sheet. At high concentrations or close proximity due to cell geometry, Na–Na interactions will factor heavily into the storage energy. At low concentrations, ionic interactions will be the main source of storage energy. This is concisely summed up in Figure 3e. Looking at the storage energy as a function of electron transfer to carbon, we see that a high voltage can be obtained without a high degree of electron transfer. Low amounts of electron transfer occur in high-concentration cells, where Na–Na interactions are prevalent. Likewise, high voltages can also be obtained with high degrees of electron transfer, which leads to strong ionic interactions. As such, we see that in the case of graphene sheets, there are two methods of Na ion storage. Either strong ionic interactions between the Na and the substrate or stabilizing Na interactions between neighboring Na atoms. However, being in the middle of these two leads to the weakest interactions. These systems are seemingly caught in a

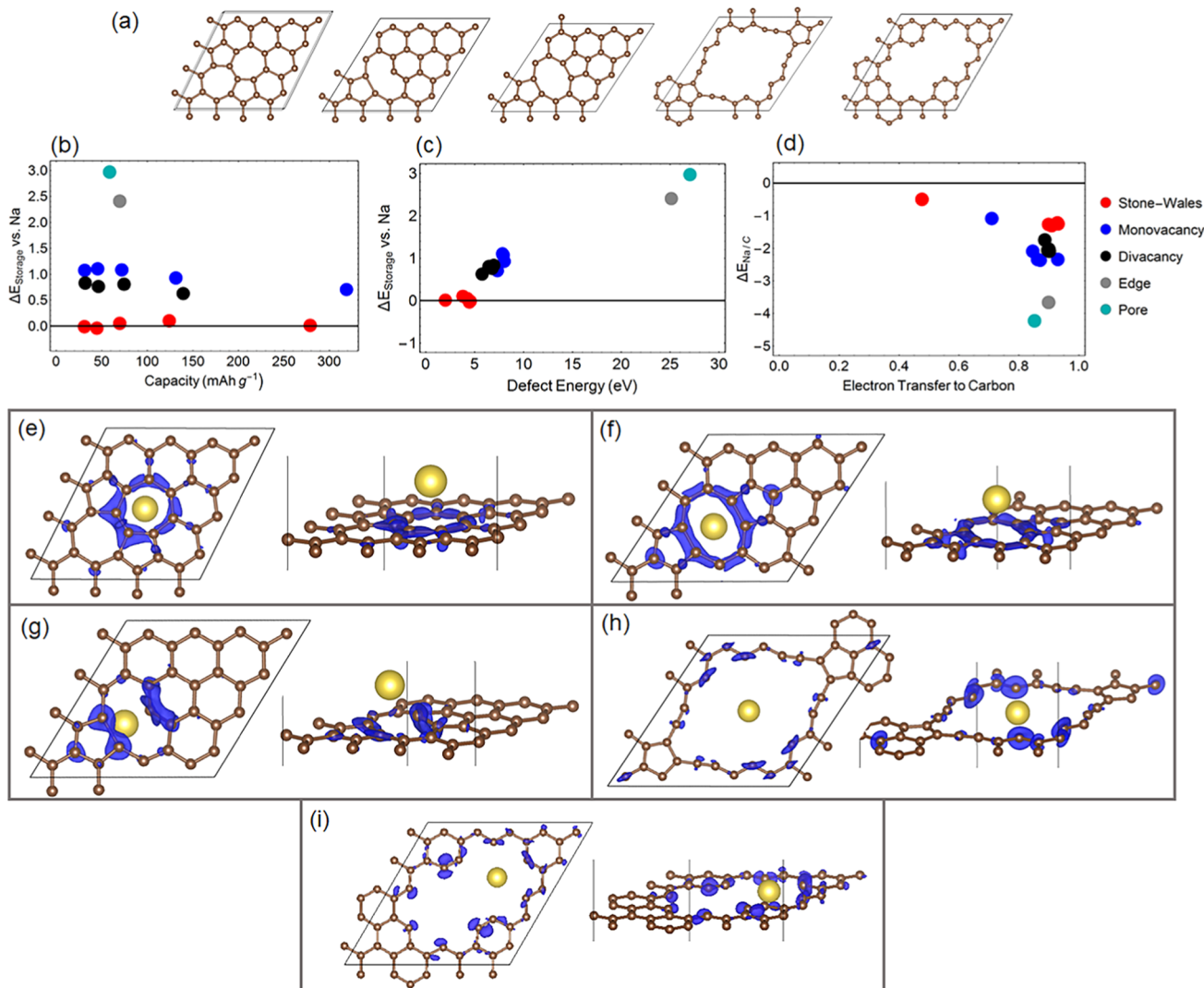


Figure 4. (a) Different types of graphene defects, from left to right: Stone–Wales defect, monovacancy, divacancy, edge defect, and pore defect. (b) $\Delta E_{\text{storage}}$ vs capacity plot of defected graphene. (c) $\Delta E_{\text{storage}}$ vs defect formation energy. (d) $\Delta E_{\text{Gr-Na}}$ vs electron transfer to the carbon substrate. Charge distribution maps showing the negative charge regions of (e) Stone–Wales, (f) divacancy, (g) monovacancy, (h) edge-like, and (i) pore-like defects.

proverbial “no man’s land”, with the unit cell being too large for stabilizing Na–Na interactions, but the degree of charge transfer being too small for strong ionic interactions between the Na and the graphene sheet.

Although these experiments show that storage on pristine graphene is never favorable, it does suggest that sodium storage at capacities close 300 mAh g⁻¹, and above, are very reliant on Na–Na interactions, as would be the case in Na–metal deposition, something that was eluded to in many of the experimental models.

3.2. Storage of Na on Defected Graphene. The previous section showed that Na concentration increases the mode of storage transitions from ionic to metallic. However, in these calculations of perfect graphene substrates, not one of the configurations was energetically favorable for sodium storage—even though they were trending that way at higher concentrations. This is not unique to our calculations; similar results have been found in numerous other DFT calculations.^{32,33,39,52–54}

However, amorphous carbon and graphene are not equivalent. Although amorphous carbon displays many

graphene-like characteristics, it also contains a high density of defects such as vacancies, dilated graphene sheets, carbon edges, and curvature. It is the presence of these defects which allow it to uptake Na in sufficient quantities to be useful as an NIB anode material. Thus, a second set of simulations focused on elucidating the interactions between sodium atoms and representative defect sites. For this task, we chose to simulate the interaction between Na and representative defect sites found in graphene sheets: monovacancy, divacancy, and Stone–Wales defects utilizing unit cells ranging from 2 × 2 to 6 × 6. Additionally, “edge” or “pore”-like defects were simulated by hollowing out a graphene sheet to differing degrees (Figure 4a).

Unlike the pristine graphene sheets, the associated storage energy relative to Na metal of most of the defected graphene sheets is favorable, and shows little dependence on the NaC_x concentration. The only exceptions are some of the Stone–Wales defects on the larger 5 × 5 and 6 × 6 sheets where the energies are slightly below 0 eV. The energy for Na storage at different defect sites is plotted in Figure 4b, which shows storage energies spanning the range of 3 eV with the majority

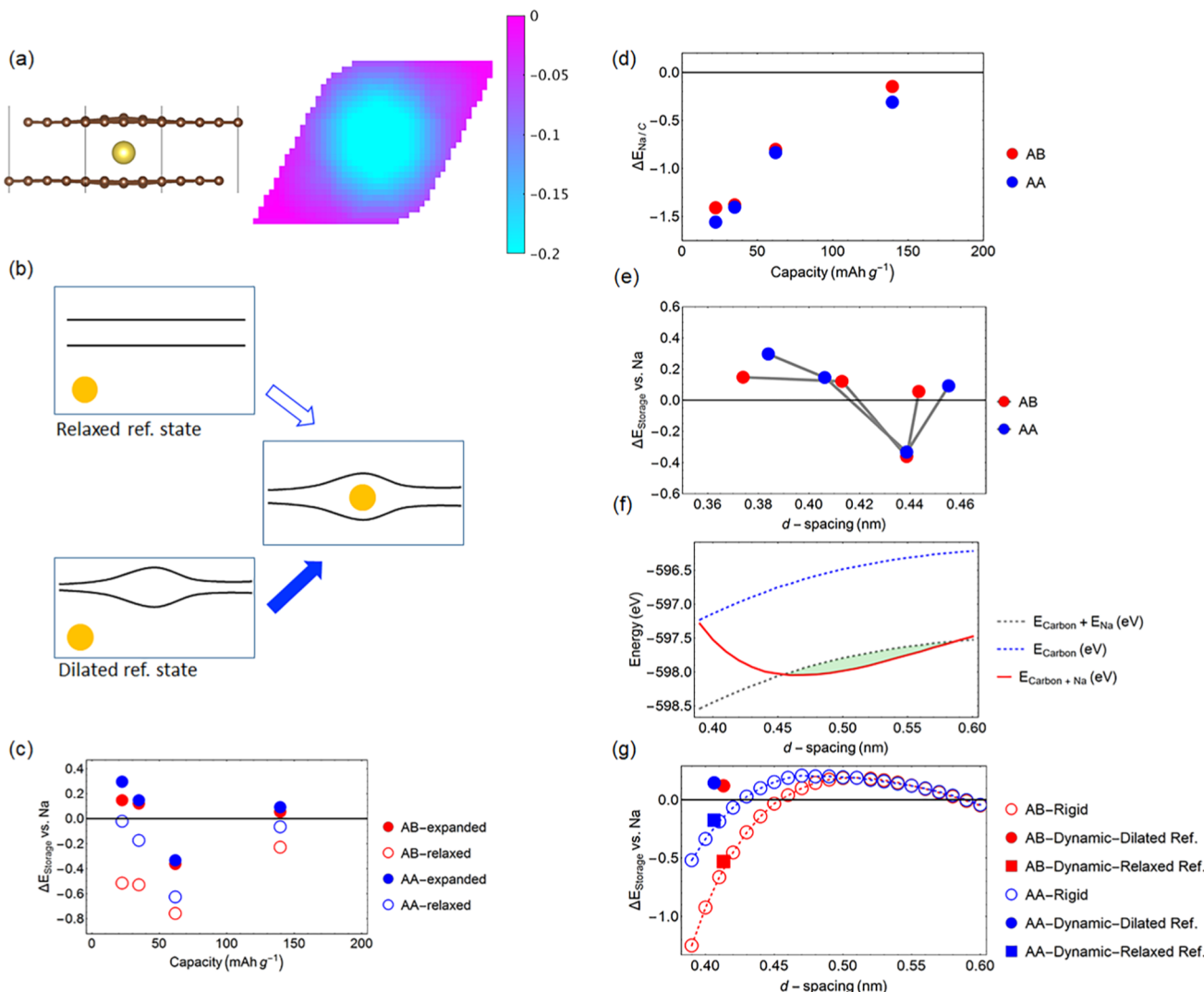


Figure 5. (a) Schematic and two-dimensional (2D) color relief map of the local vertical displacement of the lower sheet showing the bulge created by the large Na ion. (b) Schematic showing the reference states of E_{carbon} in both the relaxed reference state and the dilated reference state. (c) Storage energy vs capacity plot obtained using eq 1. Both the dilated and relaxed reference states are included. (d) $\Delta E_{\text{Gr-Na}}$, the carbon–Na interaction energy vs capacity using eqs 2 and 3. (e) Storage energy vs d -spacing plot. (f) Breakdown of the individual energies for the insertion of Na into a rigid 4 × 4-AB bilayer with a fixed d -spacing. The shaded region is where sodium atom storage is favorable. (g) Storage energies for Na insertion into 4 × 4 rigid AB and AA graphene–Na bilayers with fixed expanded d -spacings. Also, plotted is the storage energy and average d -spacing for the same sheets when they are allowed to fully relax using the both dilated, and fully relaxed, reference state.

on the order of 1 eV versus Na metal, which is suggestive of the energy scale as the sloping part of the sodiation profile in Figure 1c.

The sites on the carbon substrate most conducive to Na-storage are the edge and pore sites, though the distinction between the two open to interpretation. As such, we classify them as “edge-like” defects. Following these, monovacancy and divacancy defects are the next most favorable defects for Na storage. The energy differences between the two are small, but they do tilt towards monovacancies being more favorable. Meanwhile, the Stone–Wales defects, which possess no vacancy, are still defective enough to favor the storage of Na-atom, though they can only do so with the higher concentrations of 4 × 4, 3 × 3 and 2 × 2 graphene sheets, providing favorable storage. The trend between defects and storage energy can be concisely seen in Figure 4c, where a linear relationship between the defect energy and storage energy is observed, defect energy being defined as the

difference in energy between the defective graphene sheet and a pristine graphene sheet of similar size. As the defect energy increases, the storage energy also increases.

Furthermore, in the case of defective graphene, it can be observed that the principle factor behind storage is ionic interaction with the carbon substrate ($\Delta E_{\text{Na/C}}$) (Figure 4d). The two weakest interactions come from the 2 × 2 SW and the 2 × 2 MV substrates, due to stronger Na–Na interactions, thus showing that even when defects are involved, higher Na concentrations lead to storage, more metallic in character. Additionally, when looking at Figure 4d, we see that ionic interactions with the carbon substrate is not solely a matter of electron transfer. Aside from the 2 × 2 SW and the 2 × 2 MV substrates, all substrates show an electron transfer greater than 0.8, yet the $\Delta E_{\text{Na/C}}$ values span a range of close to 3 eV.

As such, this shows how closely binding energy and defect morphology are intertwined. As is shown in Figure 4c, more defective carbon substrates form stronger interactions with

sodium. A potential explanation for this can be given by observing plots of the negative charge surfaces (Figure 4e–i). Looking at the negative charge surfaces for hosts of different defects, with similar electron transfers, it can be seen that the concentration of negative charge varies greatly. For the SW and divacancy defect, the negative charge is spread through a more diffuse region, around a seven-member-carbon ring for the SW defect and an eight-member ring for the divacancy defect. However, in the case of the monovacancy and edge-like defects, the negative charge is gathered at local points in the carbon structure. As such, this suggests that the strength of the ionic interaction is more dependent on its distribution on the substrate, as opposed to solely the degree of electron transfer. Furthermore, this also suggests, much like an elementary concept in electrostatics, that charge prefers to gather at “sharp” points, which are typical in monovacancies and edge-like defects—features that are often described as “dangling bonds”, due to the carbon atom being bonded to only two nearest neighbors.

Returning to the interpretation of the experimental data these new computational results are insightful. First, these reveal that the presence of defects in a graphene sheet can turn an unfavorable storage environment into a favorable one. Furthermore, the more defective a substrate is, the stronger the overall binding becomes. Finally, the results also show that the interaction between the Na and the substrate is highly dependent on the substrate morphology. This corroborates experimental evidence that storage at defect sites occurs in the sloping region of the sodiation curve. Since no two defects are alike, no two storage energies at defect sites will be alike, leading to a sloping profile.

Finally, it must be noted that although some defects can provide very high-energy binding sites, it also begs the question: can sodium atoms bind so strongly to a carbon substrate that the reaction becomes irreversible? This concept was raised in a paper by Mitlin et al. who showed that not all losses in coulombic efficiency are due to the formation of the solid electrolyte interphase (SEI). There are also efficiency losses coming from irreversible trapping of sodium atoms in the structure.⁵⁵ As such, in DFT simulations, one should not only take into account whether or not the storage energy is favorable, but also whether the reaction is likely to be reversible, as is essential of a material for a rechargeable battery. For this reason, experimental approaches that focus on increasing the defect concentration should be tempered in their approach, that is, defects are good, but the proverb of having “too much of a good thing” applies here.

3.3. Storage of Na in Bilayers. Having established the storage characteristics on pristine graphene sheets and at defect sites, the third set of simulations explored the phenomenon of sodium intercalation. Experimentally, it was observed by ex situ X-ray diffraction that during sodiation of hard carbon there is a reversible dilation of the *d*-spacing between graphene layers during the low-voltage plateau of the sodiation curve.^{18,29,30,56} This implies that intercalation acts as the dominant storage mechanism in that region.

Although these experimental results show unequivocally that large quantities of Na can intercalate between graphene sheets in amorphous carbon, previous electronic structure calculations have shown that inserting Na into galleries of pristine graphite is not energetically favorable.^{9,10,57,58} However, it is also well understood that the graphene domains in hard carbon are not pristine crystallites of graphite, that is, they contain

defects, have dilated *d*-spacing, and the sheets are rumpled and sheet-to-sheet stacking is disordered. To understand how or which of these variations in the structure make hard carbon amenable to Na intercalation, we computed the energy for Na insertion versus several different reference states.

In perfect graphite, the covalently bonded carbon sheets are packed together with an AB stacking sequence, however, with the high concentration of intercalated Li this switches to an AA stacking sequence, and so in this work we compute the energy for Na intercalation into both AB and AA stacked bilayers. Calculations of flat pristine bilayers show that these structures have different equilibrium *d*-spacing of 3.35 and 3.65 Å for AB and AA arrangements, respectively.

One of our first observations from the simulations was that a single Na atom inserted into either of these structures show that the Na causes the graphene layers to bulge out-of-plane, creating a pocket for the Na atom (Figure 5a). In the case of AB starting configurations, the sheets also shift pushing them towards AA stacking. Creating this pocket involves two energy penalties, that is, the energy to pry apart the graphene layers and shift the registry, as well as the energy required to distort each of the sheets. To separate the Na/carbon interaction from the distortion penalties, we compute the energy for Na storage with reference to both flat bilayer graphene and predistorted bilayer graphene as is shown in Figure 5b. Storage energies were computed for differing concentrations of Na storage from $2 \times 2 \times 2$ bilayers up to $5 \times 5 \times 2$ bilayers, the results of which are plotted in Figure 5c.

Being a bilayer there is double the number of surrounding carbon for Na to interact with compared to monolayer graphene. Figure 5c shows that this extra interaction energy can be sufficient to overcome the cohesive energy of Na metal, but only when compared to the distorted reference state. That is, Na storage in bilayer graphene is energetically favorable if graphene is already dilated and buckled. Looking at the magnitude of the computed storage energies, all are below 0.2 eV (with the exception of the 5×5 -AA bilayer) which is consistent with the plateau region of the sodiation profile in Figure 1c. Furthermore, the difference as a function of Na concentration is small, the storage energy for a NaC_{16} AB bilayer is 0.05 eV, whereas that for a NaC_{100} bilayer is 0.15 eV implying that intercalation takes place over a narrow window of low voltages irrespective of the NaC_x concentration. All bilayers besides the 3×3 bilayer show positive storage energy. As in the other simulations, the 3×3 bilayer lands in the unstable region where the energy of the ionic interaction with carbon is diminishing (as seen in Figure 5d) but the Na concentration is not yet sufficient for Na–Na interactions to render the storage favorable.

Given that intercalation is shown to be favorable when the original bilayer structure is dilated, these results beg the question: how diluted does the bilayer need to be for favorable intercalation? And what energy penalties are harder to overcome, prying open the bilayer, or distorting the planar sheets?

Examining the computed structures of the bilayers after Na insertion, it is found that the average *d*-spacing increases with the sodium concentration, matching the experimentally measured trend. However, as is seen in Figure 5c, the storage energy is not a monotonic function of concentration. This also means that there is also not a direct correlation between *d*-spacing and storage energy as seen in Figure 5e. As such, rather than considering the *d*-spacing after insertion, a more

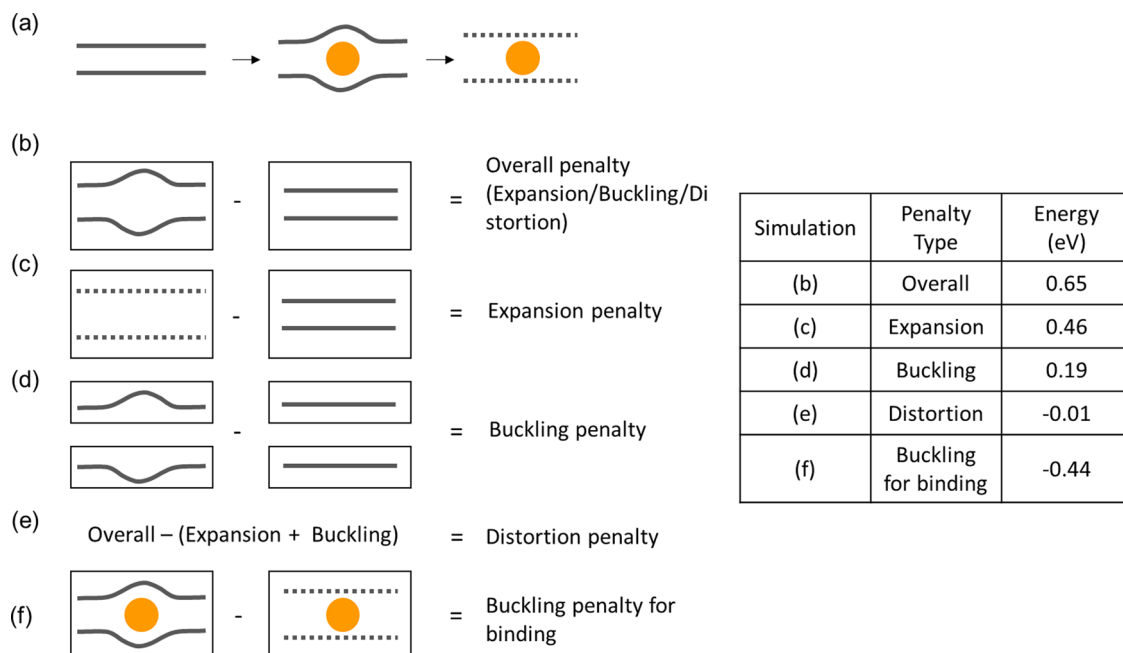


Figure 6. Calculations breaking down various energy costs of the intercalation of a Na atom in a 4×4 -AB bilayer. (a) The overall distortion penalty to create a binding “pocket” in a graphene bilayer, calculated by subtracting the energy of a relaxed bilayer from the shell of the final dilated, and buckled structure. (b) Portion of that involved in buckling sheets and (c) the portion required to expand the sheets, and buckle them to accept the sodium atom. (d) is the calculation for the Na–C interaction energy for the insertion of Na into a pocket, and (e) is the interaction energy for insertion between a pair of optimally diluted rigid sheets. In (d), the maximum d -spacing is 4.56 Å, the minimum is 3.99 Å, whereas the average is 4.13 Å. (e) The dashed lines indicate a spacing of 4.13 Å. The table on the right of the figure displays the energy cost of each of these processes and the resulting storage energies.

informative metric is the d -spacing of a bilayer needed prior to insertion for storage energy to be favorable. Hence, we performed a set of simulations placing sodium in artificially diluted rigid bilayers (Figure 5f,g) to determine the storage energy as a function of initial d -spacing.

As shown in Figure 5f, expanding a rigid AB bilayer simultaneously increases the energy of the bilayer reference state, while reducing the energy of the intercalated system. This leads to energetically favorable storage for a small d -spacing, that is, the energy of the bilayer increases, whereas the ionic interactions of the sodium and the bilayer are favorable enough to result in a positive storage energy. However, if expansion continues, the ionic interactions between the Na and the graphene sheets are no longer strong enough for a favorable storage energy.

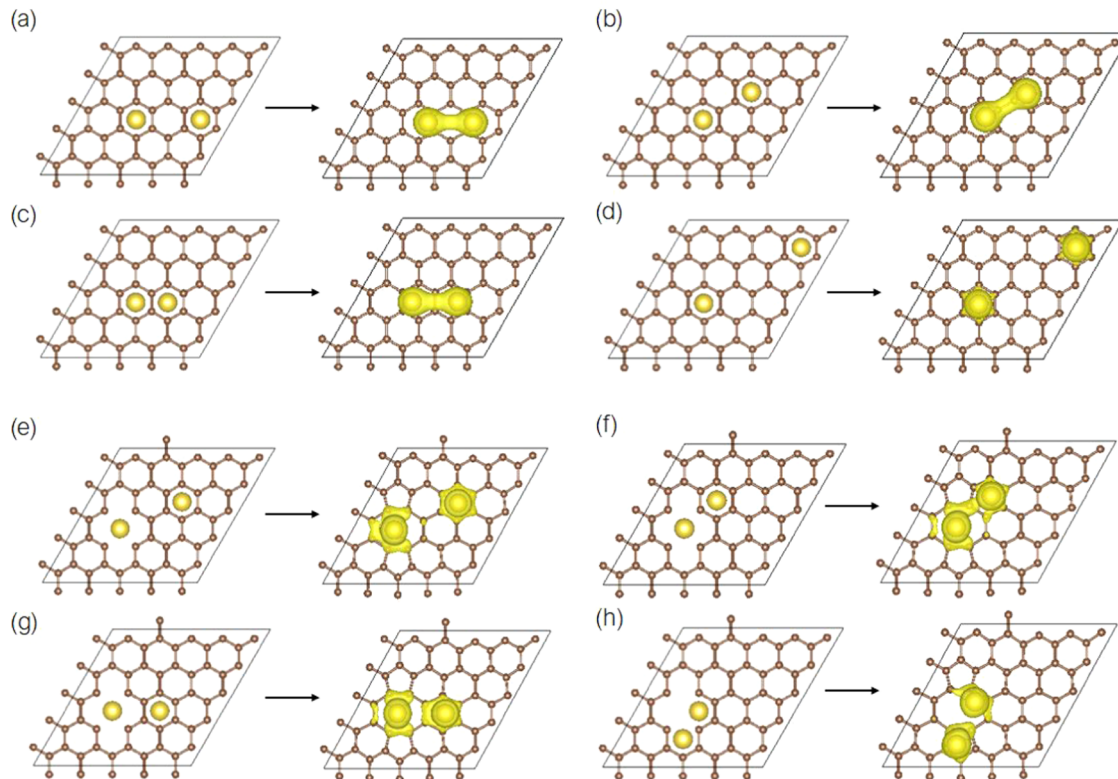
From these calculations, it is seen in Figure 5g that the minimum d -spacing needed for favorable intercalation into an AB stacked bilayer is 4.6 and 4.3 Å for an AA stacked bilayer, with most favorable Na storage at bilayers spacing of 5.1 and 4.7 Å, respectively. Also plotted in Figure 5g, the average d -spacing for bilayers that sandwich a Na atom, but are permitted to fully relax, leads to the conformal “peapod” spacing around the Na atom. These fully relaxed spacings are 4.13 and 4.07 Å for AB and AA configurations, respectively. These are average d -spacings, values that would be measured by X-ray diffraction are markedly smaller than the local dilation at Na. This provides insight into how hard carbon are able to store Na through intercalation although the d -spacings are less than 4 Å—too narrow for favorable intercalation according to the DFT results—in most hard carbon structures. In hard carbon, graphene bilayers are rippled and so the d -spacing varies with the curvature in the sheet provided local regions of large dilation are geometrically built into the structure. So, although

the average d -spacing measured by XRD is too small, there are ample local sites where Na insertion is favorable.

Although the calculations for separated rigid bilayers show that dilation of galleries is vital for favorable Na storage, the fully relaxed structure of Na inserted into a graphene bilayer shows that the Na bulges the graphene to form a pocket, demonstrating that there are several other geometric contributors contributing to the Na storage energy in the case of a bilayer.

Considering the energy terms as steps in a hypothetical pathway to forming the relaxed structure, we can consider: (i) the energy penalty to distort the individual graphene layers to form a bulge and (ii) the energy required to pry apart the graphene bilayers. These energy penalties are offset by (iii) the extra interaction energy of Na interacting with curved rather than flat graphene^{52,53} and (iv) energy changes due to shifting the registry of AB stacking towards AA stacking. To provide the direction for future experimental efforts to optimize hard carbon for Na storage, it is instructive to tease apart each of these energy contributions. Figure 6 summarizes the calculations of deconstructed and intermediate reference states performed for a 4×4 AB stacked graphene bilayer, and the resulting energy costs for each process are tabulated.

When looking at the results of Figure 6, we see that dilating the bilayer, shifting the AB registry, and buckling the individual graphene sheets (Figure 6a) incurs a penalty of 0.65 eV—which can be considered the overall penalty. However, this penalty cannot be considered to be solely a function of dilating the graphene sheets. As seen in Figure 6b, buckling both the top and bottom graphene sheets of the bilayer incurs an energy penalty of 0.19 eV. This value of 0.19 eV from distortion is comparable to the 0.13 eV of distortion energy to accommodate the intercalation of the smaller Li atom that



Substrate type	Simulation	Beginning separation (nm)	Ending separation (nm)	Storage Energy (eV)	Average electron transfer
Graphene	(a)	0.488	0.351	-0.398	0.490
	(b)	0.423	0.347	-0.413	0.467
	(c)	0.244	0.349	-0.425	0.462
	(d)	0.846	0.865	-0.557	0.659
Divacancy Graphene	(e)	0.532	0.550	0.370	0.898
	(f)	0.323	0.374	0.335	0.777
	(g)	0.366	0.384	0.274	0.787
	(h)	0.244	0.352	0.287	0.726

Figure 7. Simulation of two Na atoms on a 5×5 graphene sheet. Configurations (a–d) are on a pristine substrate, (e–h) use a substrate containing a divacancy, with one of the Na atoms bound to the defect. The storage energy and Na–Na separation results from the simulation and are displayed in a table below the figure.

was calculated by Safran et al.⁶⁰ If the graphene stack involves more than two layers there would be an additional penalty for compressing the interlayer spacing on the other side of the bulge and possibly distorting the other sheets (like the princess and the pea). Thus, the energy needed to overcome the van der Waals forces keeping the layers close, which we call the “expansion penalty”, is tabulated to be 0.47 eV.

The combination of the buckling + dilation presents an interesting case when considering the C–Na interaction. First, a buckled bilayer does not have a uniform *d*-spacing, that is the maximum extent of the *d*-spacing is on the order of 4.56 Å, whereas the minimum *d*-spacing closer to 3.99 Å. Moreover, the C–Na interaction energy invariably changes due to the distortion, with the distortion likely making the C–Na interaction more favorable. Thus, although buckling the bilayer incurs an additional penalty, it is likely that penalty can be

offset through energy gains afforded by better C–Na interactions with the buckled sheets.

In a 4×4 AB bilayer that is dilated and is hosting a Na atom in the local “pocket”, there is a storage energy of 0.12 eV, meaning that the storage of a Na atom in such a bilayer is favorable. If we compute the storage energy of a bilayer with a uniform spacing of 4.13 Å, the storage energy drops to -0.50 eV, meaning Na storage is not favorable. As such, this upends the convention of increased *d*-spacing as a method to store more Na-atoms. Two different structures with the same *d*-spacing have two drastically different outcomes, that is, the bilayer with the presence of a pocket can easily store a Na atom, the one with a uniform *d*-spacing cannot. As such, this explains the reason why hard carbon structures are so adept at intercalation. Their various defects, such as vacancies and curved sheets, leave many areas of dilated *d*-spacing in the

graphene nanodomains, with those areas being ideal for intercalation.

When further looking at the effects of intercalation in the pocket, the carbon–Na energy is of 1.38 eV with the dilated bilayer, whereas only of 0.76 eV with the rigid bilayer. This shows that the presence of uneven graphene surfaces within a bilayer help out greatly with the intercalation of a Na atom and make it possible for it to intercalate.

This is why if the sheets in a bilayer are held rigid and not allowed to buckle or not allowed to undergo transition from AB to AA or vice versa, the optimal *d*-spacing needed for a 4 × 4-AB bilayer is 5.1 Å, whereas that for a 4 × 4-AA bilayer is 4.7 Å (Figure 5f). As such, we can see that the ability of bilayers to store Na depends greatly on the local ripples and pockets that may be present in the structure—and not just on average *d*-spacing. Coincidentally, such ripples are often the result of misaligned graphene planes, along with small and defective domains, all features native to hard carbon.

As such, these results show that there is no universal answer to the question “what is the ideal *d*-spacing?” as the storage energy of intercalation depends less on the average *d*-spacing of the carbon structure, but more so on the local environment found between the graphene sheets. A very ordered and graphite-like environment without the presence of local pockets will not be favorable to Na storage, whereas a slightly defective, non-uniform *d*-spacing graphene nanodomain will be.

As such, we postulate that intercalation will be more favorable in carbons with defected graphene domains of only a few stacked layers, and in which the graphene is curved, out of registry. This structure would be most likely to be found in a soft carbon, which supports previous experimental results showing the proclivity of soft carbons to intercalate sodium atoms.^{24,61} Hard carbons, on the other, have fewer of those structures, and as such, cannot rely on the intercalation mechanism to achieve the bulk of their capacity. However, given that the individual domains in hard carbon are also defective, dilated, curved and out of registry, they should be accessible to sodium intercalation. If anything, these results show that intercalation is much more favorable if the original state of the nanodomains in the carbon are defective and dilated, as those incur a smaller energy penalty to accommodate the Na atom. As such, the results reinforce the point that graphitic materials should be avoided at all cost, since the energy penalty of opening them and buckling the individual graphene sheets to conform to the Na atom is too steep.

3.4. Dual Na Simulations. The proceeding sections discussed simulations of a single Na atom on a carbon substrate, in which the NaC_x concentration was varied by changing the number of C atoms in the calculated system. Collectively the calculations revealed two concentration affects: the accumulation of electron concentration on the carbon substrate and the interaction of sodium atoms with their images across the periodic boundaries of the computational cell. To study the interaction between unconstrained Na atoms—and to predict the theoretical maximum storage capacity of hard carbon—this section examines the interactions of pairs of Na atoms, and the next section examines clusters of multiple Na atoms.

Simulations were performed of pairs of Na atoms in different initial configurations, and we examined the energy and the final separation of the two Na atoms after the structure has been

fully relaxed. This is similar to previous work on lithium ions by Singh et al., though in their case the authors used small sheets meaning that Li–Li interactions across the periodic boundary conditions made interpreting the results difficult.⁶² To mitigate this in the calculations here, the simulations were performed using a large 5 × 5 graphene sheet. Furthermore, simulations were repeated on both a single graphene sheet as well as a bilayer, so as to ascertain any differences arising from different ionic binding contributions with the graphene sheet.

3.4.1. Dual Na on Graphene. The first set of simulations focused on Na atoms on a graphene sheet. Figure 7 shows the initial configuration for each of the calculation next to a plot of the electron density gain/loss of the final relaxed configuration. Included in the graphic is a table listing the binding energy, and the relaxed Na–Na separation. Configurations (Figure 7a–d) are for Na on pristine graphene, whereas (Figure 7e–h) are for interactions of Na where one of the Na atoms is bound to a divacancy.

Configurations (Figure 7a–d) differ in the initial separation of the Na atoms. In cases (Figure 7a–c) the atoms attract or repel so that in the final configuration the distance between the Na atoms is roughly 3.5 Å, comparable to the nearest neighbor distance of 3.72 Å in BCC Na metal, thus showing the tendency of sodium atoms to cluster together on pristine graphene sheets when allowed to break symmetry conditions. In these cases, the Na–Na interaction, which is visible in the electron density gain/loss plots, also makes storage more energetically favorable. In the case (Figure 7d), the initial configurations place one Na atom midway between the other Na atom and its periodic image. In this case, the Na atoms do not break symmetry as they relax, indicating that Na–Na interaction at this range is minimal. Looking at storage energies, the trend of more Na–Na interactions leads to more favorable storage holds true. Simulations in Figure 7a–c, which all have Na–Na interactions show greater storage energies than simulation in Figure 7d, which does not. However, as with the earlier graphene simulations, none of the storage energies suggest favorable binding, thus casting doubt on the deposition of sodium metal in pores as the last part of the sodium storage mechanism.²⁹ The simulations also underscore how important boundary conditions are within the context of DFT simulations, as these show that Na–Na interactions can occur, as long as the local Na concentration is high.

Although the calculations (Figure 7a–d) indicate that on perfect graphene–Na atoms within a certain range will be attracted to spacing of 3.5 Å regardless of orientation, the behavior on defective graphene is different. In Figure 7e–h, the Na atom on the divacancy binds with the dangling carbon bonds making it less available to interact with the second Na atom. Charge is not shared between sodium atoms, and no starting configuration relaxes to a configuration in which the Na atoms have been attracted together. Atoms which start off at intermediate and large separation distances become a little more separated, whereas atoms which start off very close together become a lot more separated. This holds true even if the distance between the Na atoms is on the order of the Na atoms on the pristine graphene sheet, as is the case for Figure 7h. This refusal to cluster together is due to the ionic nature of Na atom storage at defect sites. The large degree of electron transfer to the defect creates a positively charge Na species, which repels the other Na atom. This means that the defect sites, although very adept at storing individual Na atoms, will not act as nucleation sites for cluster formation and plating.

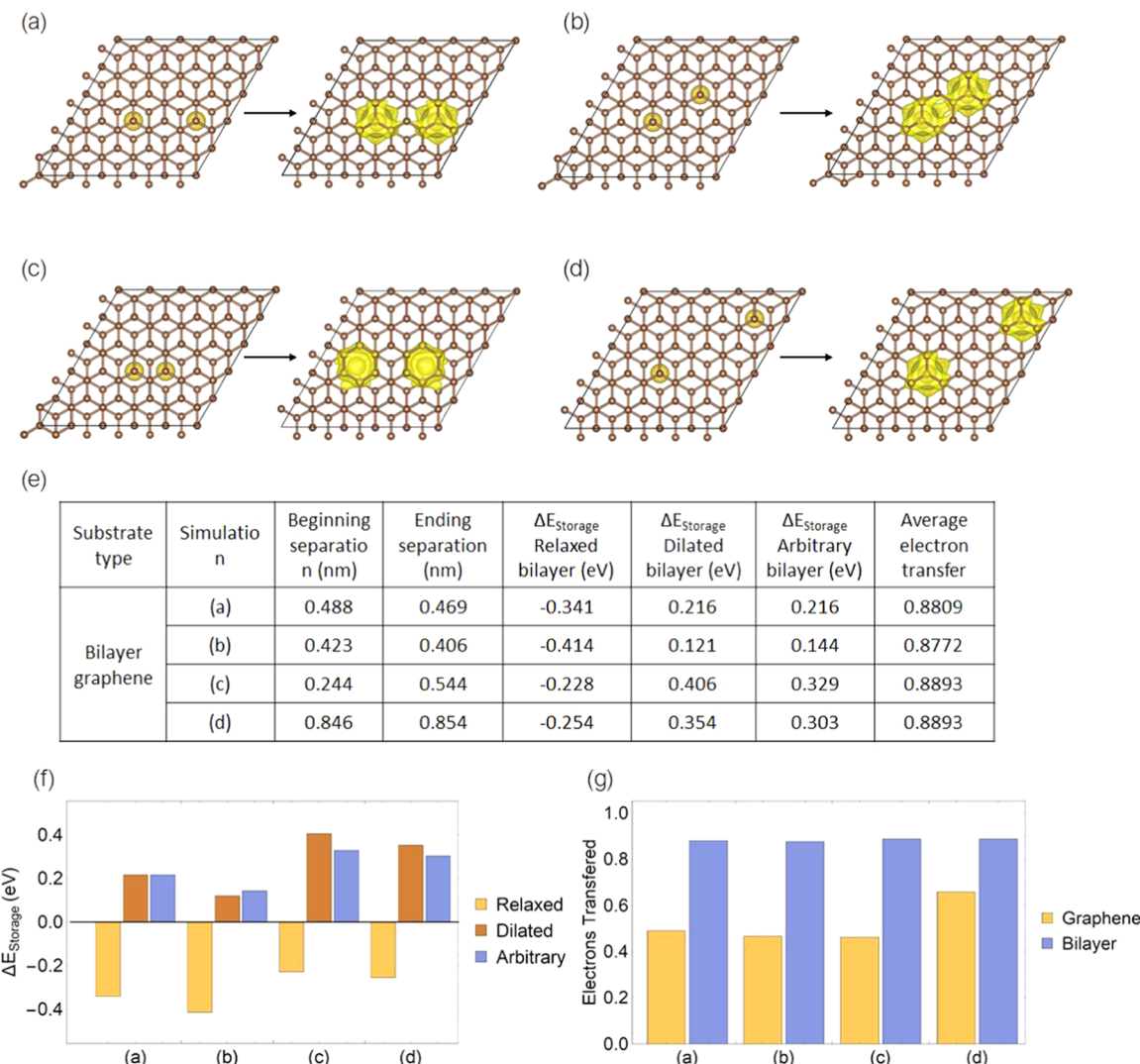


Figure 8. Simulation of two Na atoms on a 5×5 -AB bilayer, showing the before and after positions in (a)–(d). The positive charge distribution is displayed in the relaxed image. (e) Table showing Na–Na separation results from the simulation (a)–(d), storage energy vs relaxed reference state, the dilated reference state, and arbitrary dilated reference state, which was the dilated bilayer of (a), along with average electron transfer. (f) Comparison of the storage energies in (e) with the various bilayer reference states. (g) Comparison of electron transfer in (e) between the two Na on graphene, with the two Na in a bilayer.

However, it does suggest that the combination of an occupied defective site, plus a nearby atom can have a favorable storage energy, which can suggest that towards the end of the sodiation, pristine graphene surfaces already sodiated defect sites could become sodiated themselves.

3.4.2. Dual Na in a Bilayer. Simulations of Na atom pairs with the same configurations as Figure 7a–d were repeated for the Na in an AB stacked graphene bilayer. Bilayer simulations mirroring Figure 7e–h were not performed, as the presence of a defect in the bilayer would have induced a lot more complexity in teasing out final storage energies, and thus would be beyond the scope of this paper.

For these calculations, the storage energy was determined in three ways (using three different reference states of the carbon electrode). The first reference state was a relaxed 5×5 -AB bilayer and so gives the energy for insertion into a pristine graphitic gallery. The second was versus the bilayer in its final relaxed structure when hosting the Na, and so this yields just the Na/C interaction energy of each configuration. To enable comparison of the different Na configurations, the third

storage energy computed is versus a common dilated reference state, which in this case was the dilated sheets in Figure 7a. The reason was the comparison with the arbitrarily dilated bilayer, because we wished to focus on the ideal Na–Na spacing, and as such, did not want to convolute results with that of extremely dilated bilayers, where the storage energy is more a function of the defectiveness of the bilayer, as opposed to the Na–Na spacing. Finally, even though a 5×5 bilayer has 100 carbon atoms, capacities were calculated with respect to 50 carbon atoms, as we assume the bilayer to be representative of an infinite stack, as is described in Section 4.

Unlike the results seen with the single graphene sheet, the Na atoms in the bilayer show a reticence to cluster with each other (Figure 8a–d). Unlike the two Na atoms on a graphene sheet, which settle at a distance of roughly 3.5 Å of one another, the pair of Na atoms in a bilayer show little movement from their starting positions. The inter Na distances in calculations (Figure 8a,b,d) are very close to their initial distance, with the closest distance being of 4.1 Å, as seen in Figure 8b. Furthermore, the Na atoms in simulation (Figure

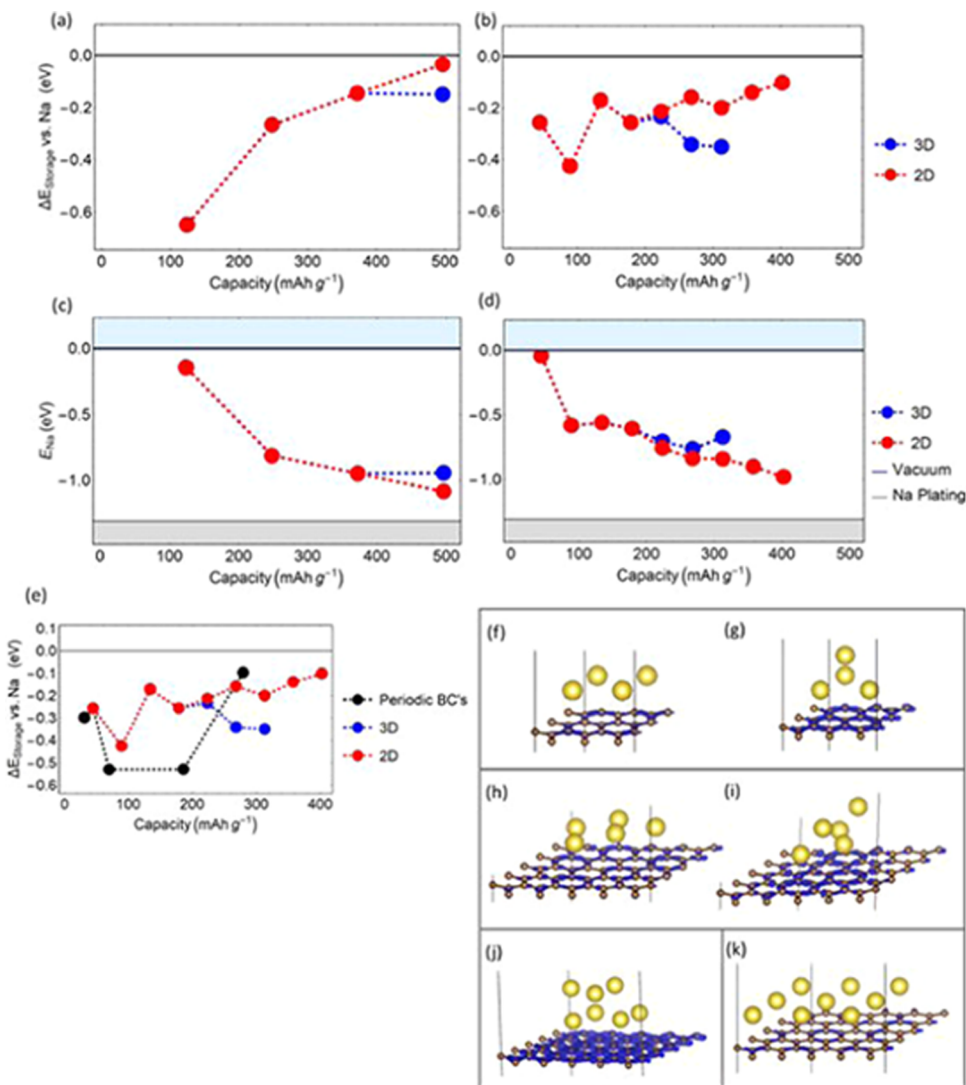


Figure 9. Storage energy vs capacity plots of multiatoms depending on geometrical arrangement for (a) a 3×3 graphene sheet (b) a 5×5 graphene sheet. Average E_{Na} for the (c) 3×3 graphene sheet, (d) the 5×5 graphene sheet. (e) Storage energy vs capacity plot comparing the effects of increasing capacity by using a smaller unit cell, thus decreasing Na–Na distances across boundary conditions, and adding more Na atoms to a 5×5 graphene sheet. Negative electron density gain/loss plots for the (f) 2D 3×3 graphene sheet, (g) 3D 3×3 graphene sheet, (h) 2D 5×5 graphene sheet, (i) 3D 5×5 graphene sheet, (j) 5×5 graphene sheet with seven sodium atoms, originally in a 2D configuration, (k) nine sodium atoms in a 2D configuration.

8c), which started in close proximity to one another, show much greater final relaxed separation than their counterparts did on the single graphene sheet. The Na atoms in the bilayer separated to a distance of over 5.4 Å, whereas the Na atoms on the single graphene sheet separated to a distance of 3.5 Å.

It is curious that the Na atoms in Figure 8c which started closer together, end further apart than the atoms in Figure 8a,b, which started further apart. Upon closer inspection of the structures, we see that the Na atoms in Figure 8c end up over a hexagonal site in the bottom layer and under a bridge site of the top layer. Meanwhile, the Na atoms in Figure 8a,b end up in a hexagonal site/top site combination. Bader charge analysis reveals that, in the hexagonal/bridge configuration, the Na/C interaction is more strongly ionic than the hexagonal/top configuration, which would explain the more distant separation. Additionally, it is likely that the proximity of the Na atoms in Figure 8c at the onset was far from equilibrium, and the relaxation path from this configuration avoided the

local energy well in that trapped the relaxation of initial configuration (Figure 8a).

In all four of the configurations computed for two Na atoms in a bilayer, the predicted storage energy was positive, which is favorable with respect to the reference configuration, and shows a direct correlation with the final Na–Na separation; the larger the separation the more energetically favorable the storage. This indicates that it is unfavorable for Na atoms intercalated into bilayers graphene layers to dimerize—the opposite of what is seen on a single layered graphene substrate. The storage energies for the bilayer configurations (Figure 8a–d) are favorable relative to a dilated bilayer, but they are negative (unfavorable) for insertion into a nondilated bilayer. However, in each case the Na–C interaction energy in the bilayer configurations is considerably larger in their counterpart monolayer configurations.

Furthermore, there is little difference between the storage energies computed versus the dilated reference state, and the arbitrarily diluted reference state. This means that the

difference in storage energies is less because of an increased defectiveness—since we consider dilated and buckled bilayer to be defective structures—as was seen in *Figure 4c*, and more due to an increase in ionic interactions between the Na and the carbon, which is afforded by the greater spacing. Smaller spacing between the Na atoms lead to less favorable interactions, as they begin to get closer to Na plating.

The changing nature of the interactions going from ionic to metallic is seen with the Bader charges in *Figure 8a–d* showing a larger charge transfer from the Na, and so larger iconicity in the bilayer interaction—the ability to distribute charge over a more enclosing shell of C lowers the energy of the ionic electronic configuration and so suppresses the Na–Na metallic interaction seen on the bilayer. This stronger ionic interaction on the bilayer explains the larger preferred Na–Na spacing in the bilayer, but it also reveals that the onset of the Na–Na metallic interaction is due to competition with Na storage, and the extent to which monolayer graphene can be used as a model for the complex structures of hard carbon.

3.5. Multi-Na Simulations. The calculations of two Na atoms in the preceding section revealed the changes in Na storage energy with the Na–Na spacing at a fixed state of charge. These revealed that on monolayer graphene–Na will forgo ionic interaction with graphene in favor of forming a metallic Na–Na dimer, but the fact that the additional carbon interaction available in the bilayer suppresses this. This section examines the favorability of Na storage in a Na cluster as the Na concentration is increased. This includes the preference for two-dimensional (2D) versus three-dimensional (3D) clusters growing both on an unconstrained graphene substrate and within a graphene bilayer. Simulations were performed of three or more Na atoms on 3×3 and 5×5 pristine graphene substrates, arranged initially either in a single 2D layer or in a 3D cluster. Na was added iteratively, relaxing the structure with the new Na atom before adding the next Na.

3.5.1. Multi-Na on Graphene. The results for Na on the single graphene sheet are shown in *Figure 9a,b*, plotting the storage energy as a function of concentration on the 3×3 and 5×5 computational cells respectively with the atoms arranged initially as a 2D island (red), or as a 3D cluster (blue). The storage energy is not energetically favorable, but it moves towards being more favorable as more Na is added. During this process the Na clusters undergo transition to reassemble Na–metal more than a carbon–Na compound, as is shown by the average energy of the sodium atoms in the respective clusters (*Figure 9c,d*), which increasingly trend towards the value of Na in its BCC unit cell. For Na storage, this suggests that at voltages close to that of sodium metal, sodium atoms might be stabilized in large part due to metallic interaction or could adopt a storage energy provided there is a weak ionic interaction from a slight defective graphene sheets, which was also suggested in the two Na atom simulation on a divacancy defective sheet. This is also similar to observations made by Singh et al. who also performed comprehensive calculations on Na-clusters on a graphene sheet, and found weak ionic interactions between clusters and the graphene substrate, but progressively more stable interactions as the concentration of sodium atoms in the cluster increased.⁶³

The storage energy is not monotonic during the transition from predominantly ionic to predominantly metallic bonding. The dip storage energy near 100 mAh g^{-1} in the 5×5 graphene sheet corresponds to two Na atoms on the substrate (*Figure 9e*). At this initial stage of clustering the graphene's

ability to withdraw electrons is saturated and so the ionic interaction has to be shared by both Na atoms, but there is insufficient Na–Na interaction from just two atoms offset the reduction in ionic binding. As such, this corroborates experimental observation that show Na-metal deposition can only occur at higher sodium concentrations and not in isolated clusters at the beginning of sodiation. Once the concentration is increased to three Na atoms and beyond, the voltage, albeit never being positive, begins to rise as long as the sodium is initially placed in a 2D configuration.

We can also see from *Figure 9e* that the cluster calculations show the storage energy is more favorable when the Na is initially arranged as a 2D layer. The final relaxed structures of the systems that started off as 2D layers have both a larger Na–C interaction and larger Na–Na interaction than the relaxed structures that started off as 3D clusters. Furthermore, it also shows the disparity between storage energies when multiatom simulations are used to increase the concentration, as opposed to single atom simulations with a shrinking unit cell size. Multi-Na atoms simulations on a 5×5 graphene sheet in the $100\text{--}200 \text{ mAh g}^{-1}$ concentration showing much higher voltages, than equivalent simulations single sodium atom on a 3×3 and 4×4 graphene sheet—thus showing the importance of considering boundary conditions when trying to interpret results with higher Na concentrations.

Figure 9f–k delve further into the multiatom simulations observing the different nature of the charge transfer between the sodium clusters and the graphene sheet. The 3D clusters show strong electron transfer to graphene from the “base” sodium atoms, thus increasing the ionic interactions. However, the “top” sodium atoms are not connected to the sheet and become negatively charged, creating a screening layer to compensate the positively charged Na below. The 2D configuration is completely different. It has only partial electron transfer to graphene, making weak ionic interaction, but more in plane metallic bonding. This is seen both in the case of the 3×3 and 5×5 graphene sheets.

Up to now there are six sodium atoms on the sheet, the 2D arrangement is preferred as opposed to the 3D one, with the same charge screening being observed, with the greater negative charge concentration on the graphene with the 3D configuration being in evidence in *Figure 9i,j*. However, for seven carbon atoms, the 2D configuration is no longer stable, that is, the starting initial 2D arrangement spontaneously relaxes to a 3D cluster. The instability for a seven-atom cluster is surprising as seven is typically a magic number for 2D islands on a triangular lattice. Regardless, this would mean that clustering, and thus plating would begin at a concentration of Na_7C_{50} , which is equivalent to a capacity of 312 mAh g^{-1} , making this a theoretical limit of capacity—which is not too far from what is observed experimentally!

However, there are a few issues with this observation. First, the arrangements preceding the Na_7C_{50} arrangement never showed a positive storage energy. Furthermore, the larger eight and nine atom clusters remained stable as a 2D layer. These larger clusters are probably stabilized as 2D layers by interactions across the periodic boundaries of the computational cell and cannot break the arrangement. This was also the case with four sodium atoms on a 3×3 sheet. As such, the results of clustering versus nonclustering is too affected by the boundary conditions for us to make strong conclusions going off of this data alone.

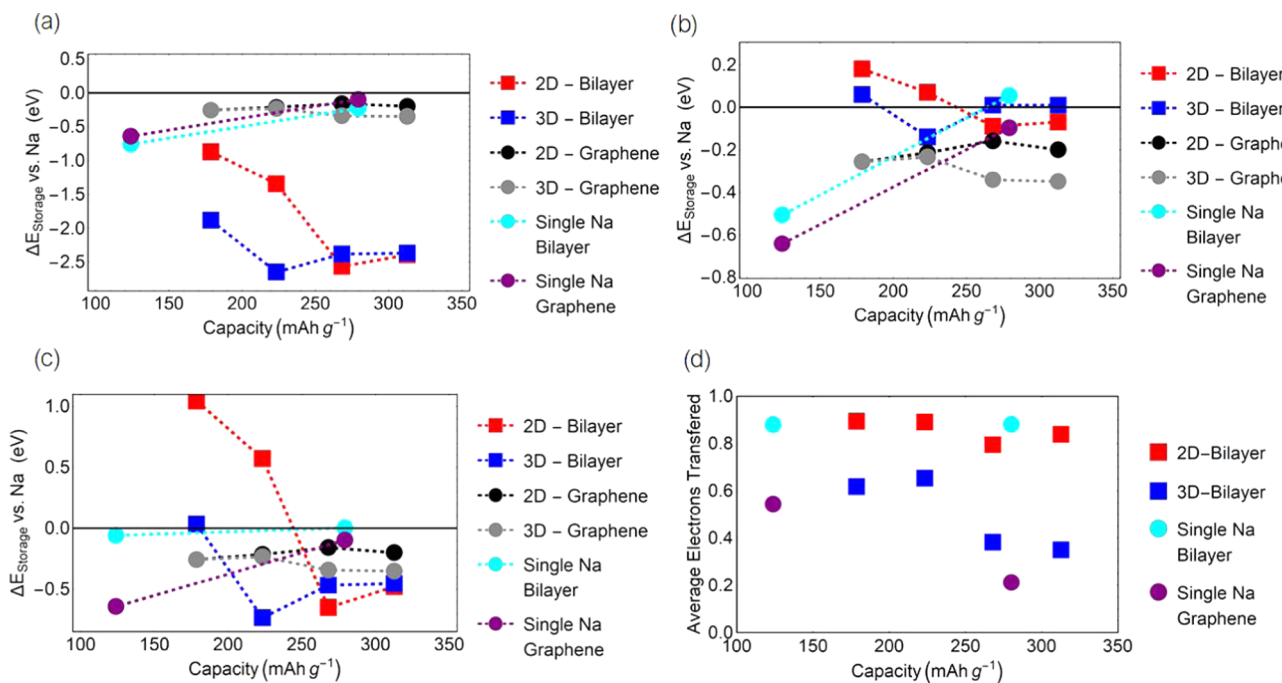


Figure 10. Storage energy comparison between multiple sodium atoms stored on a single graphene sheet in a 2D/3D arrangement and sodium atoms in a bilayer on a 2D/3D arrangement. Also, added for comparison are the results of a single Na atoms in the 2×2 -AB and 3×3 -AB bilayers, and a single Na atoms on the 2×2 and 3×3 graphene sheets. This is to juxtapose the ideal spacing, with that of the multiatom spacing. For the bilayers, the storage energies use as a carbon reference state (a) a relaxed bilayer. (b) The dilated bilayer at the end of the respective simulation. (c) an arbitrary dilated bilayer, which in this case was the bilayer at the end of the seven Na-2D simulation. (d) Electron transfer between the sodium 2D and 3D clusters to the bilayer, as well as those for the single Na atom in 2×2 and 3×3 bilayers, along with the 2×2 and 3×3 graphene sheets.

3.5.2. Multi-Na in a Bilayer. As with the two Na atom calculations, the calculations of the multiple Na clusters on monolayer graphene were repeated for AB bilayer graphene. These calculations reveal that the presence of an additional graphene sheet affects the cluster formation and electronic structure of the Na cluster–carbon interaction. These calculations were performed with four to seven Na atoms placed into a dilated 5×5 AB bilayer, either in a 2D or 3D arrangement. The dilation at the outset was the same for both the 2D and 3D structures, so as to give equal opportunity for the atoms to agglomerate or to spread out and conform to the substrate. As with the two Na simulations in a bilayer, the storage energy was computed with respect to a common carbon reference structure of a dilated bilayer, and Na–C interaction energy is given by using as a reference state of the final relaxed deformed carbon configuration for each individual cluster. The capacities are computed assuming an infinite stack of bilayers, effectively halving the NaC_x stoichiometry, and thus doubling the capacity.

The initial and relaxed structures are shown in Figures S3–S6 (Supporting Information), along with information about the degree of electron transfer from each Na-atom to the graphene bilayer. Upon relaxation, the initially 3D four and five atom clusters spread out to wet the substrate as a 2D layer. The initially 2D and 3D structures of the six- and seven-atom clusters, on the other hand, remained as distinct 2D and 3D arrangements after relaxation.

The storage energy per Na atom is plotted for all the clusters in Figure 10a–c. Using the reference state of a relaxed 5×5 bilayer, all of the storage energies are extremely negative and much more so than the equivalent Na concentration represented by a single Na atom in a smaller bilayer. As

such, this shows that the “ideal” system is an evenly spaced 2D one—though ideal systems may not be an accurate representation of reality. Furthermore, multiatom storage is much more favorable on a graphene sheet, which shows that if clustering were to occur, it would be on a graphene surface, and not in a bilayer.

Using the dilated bilayer found at end of the simulation provides more interesting results (Figure 10b). It can be seen that for the case of four and five Na atoms clusters, which occupy the capacity window between 200 and 250 mAh g⁻¹, the 2D cluster configuration is most stable, but that larger clusters show a drop in the per atom storage energy and with 2D and 3D clusters becoming very similar in energy. This is inline with the storage model that attributes the low voltage plateau below 0.2 V to intercalation. Furthermore, even though the 3D arrangements manage to spread out into 2D configurations, they do not manage to find a structure with as low an energy as the relaxed structures that started off in a 2D arrangement. This suggests that under ideal conditions atoms will, until a certain point—which in this case is close to 250 mAh g⁻¹—prefer to be stored in a 2D arrangement.

The simulations with six Na atoms and seven Na atoms, which represent capacities in the 250 mAh g⁻¹ range to 320 mAh g⁻¹ range offer slightly different results. In these cases, the 3D initial arrangement is most stable after relaxation, with both of the simulations showing a storage energy per Na of 0.01 eV. This tells us that if a bilayer is diluted enough, and sodium atoms are initially arranged as a 3D cluster, favorable storage is in fact possible. Furthermore, the preference of the Na atoms for a 3D cluster over a 2D arrangement at high concentrations is the case here, the ideal case is still a 2D configuration. When the storage energy of a single Na atom in a 2×2 -AB bilayer,

which when making the infinite bilayer approximation has a stoichiometry of NaC_8 , the storage energy is more favorable than comparable concentration of multi-Na atoms on a larger patch. As such, under theoretical conditions, a 2D arrangement will still be preferred—however, such theoretical conditions are poor approximators of real-life systems, and as such, multi-Na atoms on larger carbon substrates are much more appropriate.

However, a caveat with the storage energies obtained using the dilated bilayer as a reference state is that the bilayer can unduly influence the final energy. As such, we used an arbitrarily dilated bilayer as a reference to check whether the 2D or 3D multi-Na configuration was the most stable (Figure 10c). As was alluded to in Figure 10a,b, the 2D configuration with four Na and five Na atoms is more stable than the 3D configuration, whereas the 3D configuration is more stable with six Na and seven Na atoms. Furthermore, the single Na in the 2×2 bilayer showed a higher energy than all the multi-Na simulations, which further goes to show that evenly distributed Na atoms in a 2D arrangement are the most stable.

Looking further into the results through analysis of the Bader charges (Figure 10d), we see that the 2D arrangements have a much high average of transferred electrons than the 3D arrangements. Like the dual Na simulation in a bilayer, this suggests that the 2D sodium atoms are stored primarily through ionic interactions, which is favorable, as long as there is enough space for Na atoms to avoid repulsive interactions from each other. What is interesting is that, even at higher Na concentrations, the average electron transfer of the 2D arrangement does not experience a steep drop, meaning that the storage is still reliant on ionic interactions—despite the presence of more Na atoms. This does not occur, which supports the conclusion from the previous paragraph, stating that metallic clustering is unlikely to occur in a bilayer.

The Bader charges of the 3D configuration do show a change in pattern. In the case of four Na and five Na, the degree of electron transfer is lower than that of the 2D configuration, but still high enough to promote ionic interactions. This explains why the storage energies are lower than those of the 2D configuration. However, the degree of electron transfer with the six Na and seven Na simulation experiences a steep drop, whereas the average was 0.62 and 0.65 for electrons transferred for four and five Na clusters, and the average electron transfer for six and seven Na clusters was 0.38 and 0.35, respectively. This implies that at around six or seven Na atoms clusters (at this NaC_x ratio) undergo a dramatic transition shift to a metallic type storage. This degree of electron transfer is similar to the one seen by a lone Na atom on a 2×2 graphene sheet—which we ascribed to be metallic dominated storage earlier on in the paper.

Furthermore, when looking at the individual electron transfers (Figures S5 and S6, Supporting Information), we see that the electron transfer varies widely between certain Na atoms, with some showing a high degree of electron transfer and others close to none at all. As such, this shows that the 3D clusters at these concentrations can be stored through a mix of metallic interactions with the atoms in the center of the cluster as well as ionic interactions with the atoms closer to the graphene sheets of the bilayer. Finally, it must be noted that, under the single Na configuration in the 2×2 bilayer, the degree of electron transfer is higher than in the multiatom simulation, thus explaining the more favorable storage energy

as well as the proclivity for ionic storage under theoretical conditions.

Though this shows that clustering in bilayers can be favorable, the conditions necessary to lead to this are highly unlikely, that is, a highly diluted bilayer, along with a 3D initial configuration. In actual experimental conditions, this is rather unlikely. Graphene sheets are seldom this diluted, and there is no such thing as the “initial 3D configuration”. However, the results could be extrapolated to the type of storage present in micropores. Due to curvature, certain micropores could well be considered as diluted bilayers. Furthermore, micropores that contain defect sites could initially store Na atoms in a cluster-like arrangement through ionic storage, before switching over to metallic storage later in the last steps of sodiation. Such a process, would fit well with the experimentally determined storage model, which puts near-metallic storage in pores and on graphene surfaces as the last step before plating—something which is alluded to in these simulations.

4. ON THE NATURE OF A THEORETICAL LIMIT

Factoring the multi-Na simulations with the rest of our results, we can begin to close in on a theoretical limit for hard carbon materials. As such, we will make two separate arguments for a capacity limit, one based on geometry obtained from the two Na simulations and the other based on the clustering behavior of Na atoms, seen from the multi-Na simulations.

4.1. Geometric Capacity Limit. This limit focuses on a geometric argument. This is able to be justified, as we were able to show with the multi-Na simulations that the most favorable storage energies, both on graphene and in a bilayer, were obtained from evenly spaced Na atoms. However, determining the capacity by using a single Na atom and changing the size of the graphene sheet does not allow us to gage an accurate equilibrium distance. As such, we used equilibrium distances between dual Na atoms on a graphene sheet and in a bilayer to posit a theoretical capacity limit.

Looking back to the two Na simulations on the 5×5 graphene sheet, we see that the minimum distance between the Na-atoms settles to around 3.5 \AA . From knowing such a distance, we can create a theoretical unit cell around the Na atom and transfer it over an infinite graphene sheet. Since we know the theoretical surface area of graphene on one side to be $1300 \text{ m}^2 \text{ g}^{-1}$, we can then estimate the number of Na atoms per gram from an area calculation using the equation

$$\frac{1300 \text{ m}^2 \text{ g}^{-1}}{x(x \sin\left[\frac{\pi}{3}\right])} \times F \times \frac{1000 \text{ mA}}{A} \times \frac{h}{3600 \text{ s}} = \text{mAh g}^{-1} \quad (8)$$

where x is the Na–Na distance in meters, $x(x \sin(\pi/3))$ is the Na unit cell area, F is faradays constant, and $1300 \text{ m}^2 \text{ g}^{-1}$ is the surface area of graphene. The rest of the terms are conversion factors. Under such assumptions, sodium atoms spaced 3.5 \AA apart would have a capacity of 543 mAh g^{-1} . If sodium atoms were stored on both sides, the capacity would be doubled to 1086 mAh g^{-1} .

Unfortunately, we also know from the previous simulations that storage on graphene on one side, let alone two, is never favorable. However, storage in a bilayer is favorable. As such, we can hypothesize that for every layer of sodium atom, there needs to be two layers of graphene, thus leading us to add a $(N - 1)/N$ constant

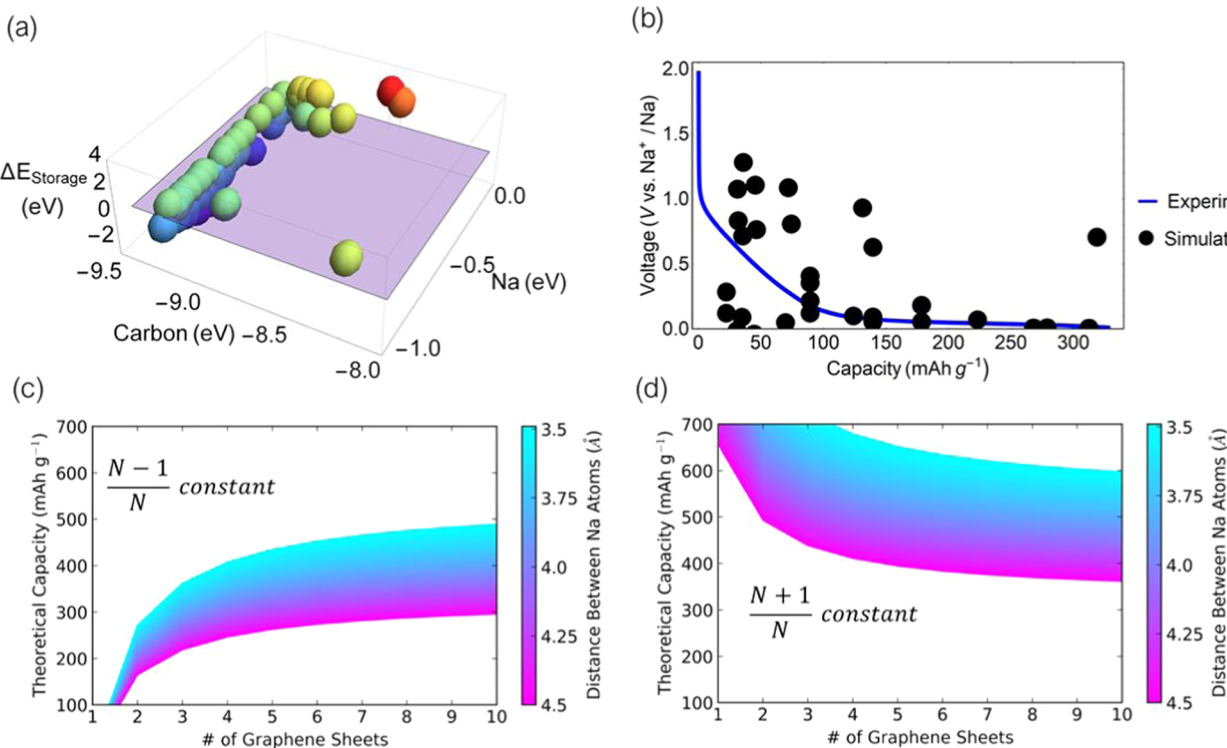


Figure 11. (a) Three-dimensional summary plot of all the simulations. The x axis is a measure of the Na unit cell energy, with more negative values implying more metallic behavior. The y axis is a measure of the average carbon energy, with the higher, less negative, numbers indicating more defective carbon substrates. The z axis is the storage energy in eV, with the plane representing the 0 V favorability threshold. (b) Plot an actual charge/discharge curve, with all of the simulations with a final storage energy above 0 eV as a function of capacity. V vs Na^+/Na is used as a reference state. (c) Theoretical capacity plot using the approximations made in eq 9. (d) Theoretical capacity using a $(N + 1)/N$ constant in eq 9.

$$\frac{1300 \text{ m}^2 \text{ g}^{-1}}{x(x \sin[\frac{\pi}{3}])} \times F \times \frac{1000 \text{ mA}}{\text{A}} \times \frac{\text{h}}{3600 \text{ s}} \times \left(\frac{N-1}{N}\right) = \text{mAh g}^{-1} \quad (9)$$

where N is the number of layers of graphene. Adding this constant and plotting it for a typical hard carbon with layered domains of three to five graphene sheets, we see the theoretical capacity to be 365 mAh g^{-1} for three layered domains and 434 mAh g^{-1} for five layered domains (Figure 11c). More domains would mean the capacity would eventually asymptote to 534 mAh g^{-1} , however, more domains would also imply a more graphitic structure, which would become more and more unfavorable to intercalation. This theoretical capacity is similar to a recent one proposed by Searles et al. which found it to be either 360 mAh g^{-1} for a single-side graphene sheet binding or 551 mAh g^{-1} for a double-side graphene binding.⁶⁴ However, it is important to mention that the basis for their model was one of “sheet disruption” and that their model also included hydrogenated graphene sheets. Should one make the assumption that graphene sheets store on both sides, the constant would be changed to $(N+1)/N$ —though this type of binding has not shown to be feasible (Figure 11d).

However, the work done looking at the two Na simulations in bilayers showed that distances between two Na atoms in bilayers are greater than those on graphene sheets, due to greater ionic interactions with the graphene and, as such, more ionic repulsion from Na atom to Na atom. If the Na to Na minimum distance is to be considered as 4.1 \AA and plugged into eq 8, a maximum capacity of 396 mAh g^{-1} is obtained from a single sheet. Using the domain approximation in eq 9,

this theoretical capacity drops to 300 mAh g^{-1} . Of course, this capacity does not take into account storage at defective sites or metallic storage—but it does come very close to observed experimental values.

4.2. Clustering Capacity Limit. The other argument that can be made for capacity limit is one of clustering. Even though a 2D arrangement is the most ideal, that is, unlikely to occur in an actual system. As we saw from the multi-Na simulation on larger sheets, there was a tendency of Na atoms to show more favorable energy in a 3D cluster as opposed to a 2D arrangement after a certain concentration.

In the format of the “rocking-chair battery”, which a NIB is, a full sodiation is considered to be the number of atoms that can be inserted into the carbon and on its surface without reaching the Na-plating regime. When looking at the multi-Na simulation on a 5×5 graphene sheet and on a 5×5 bilayer, both cases showed stable 2D growth until six to seven Na atoms were placed.

Up until that point, the sodium had followed Stranski–Krastanov growth and spread out over a 2D surface before beginning to cluster. On the graphene sheet the seven Na atom simulation with an initial 2D configuration rearranged into a 3D configuration. With the case of the multiple sodium atoms in the 5×5 bilayer, the same thing was observed, that is, 2D growth was more favorable until six Na atoms were reached. At six atoms, the 3D configuration was more stable and also showed a much lower degree of electron transfer to the graphene bilayer, meaning stronger metallic interactions, which is a prelude to sodium plating. For the seven Na atoms, the degree of electron transfer was even less, thus giving even stronger suggestion of metallic behavior. Whether this type of

metallic behavior should be classified as Na-metal plating or one of the myriads of names, such as “clustering”, “under-potential deposition”, “storage in pores”—all names that suggest plating is imminent—is debatable, and cannot be solved in the context of this paper alone. As an aside, we stipulate that “near-Na metal plating” might be a more appropriate term that can cover many ambiguities. However, the data does suggest that in the case of amorphous carbon, near-plating/plating behavior occurs at a ratio close to $\text{Na}_6\text{C}_{50}/\text{Na}_7\text{C}_{50}$, which is equivalent in capacity to 268–312 mAh g⁻¹.

5. CONCLUSIONS

In this article, we presented the synthesis of a large number of DFT calculations of Na interacting with graphene substrates, ranging from pristine graphene, defects, bilayers, and multi-Na atom simulations. These revealed that there are two regimes of Na atom storage on carbon. The first one is through ionic storage, either due to a defect substrate or a storage in the bilayer. The second is through Na–Na metallic interactions, which occur when Na atoms are in close proximity to each other. This trend is clearly seen on the 3D summary plot (Figure 11a), which shows the two main trends. Ionic storage via defects proves to be favorable, whereas the metallic interactions help storage in the case of bilayers and slightly defective structures, but are not strong enough to induce storage of sodium atoms on pristine graphene. There is just one lone outlier that expresses a high carbon defect energy, along with a high Na energy—this being the Na on a 2 × 2 graphene sheet with a monovacancy defect—an experimentally implausible structure.

These results regarding the defects and bilayer intercalation are very similar to that what was experimentally elucidated by Mitlin et al.,¹⁷ Ji et al.,²⁹ Tarascon et al.,³⁰ and Grey et al.,³¹ and the amalgamation of all simulations leads to a shaped suggestive of the slope/plateau curve as seen in Figure 1c (Figure 11b). Regarding the storage mechanism of sodium deposition often reported in many papers, these simulations neither confirm nor deny it. Indeed, it is showed that higher Na atom concentrations exhibit metallic binding behavior, but such behavior is not favorable enough to be able to store these atoms on pristine graphene sheets. It is likely that the last part of the experimental sodiation curve right before Na plating is due to sodium storage at very weak defective sites on the graphene, such as Stone–Wales defect, also aided by metallic interactions with surrounding Na atoms.

Finally, we also utilized the trends seen in our many simulations to hypothesize the existence of a theoretical capacity limit with a geometrical argument and clustering argument. The geometric argument places the capacity in the 300–400 mAh g⁻¹ region, whereas the clustering argument is near the 300 mAh g⁻¹ region. Of course, these theoretical capacity arguments do not take into account defect sites and cannot differentiate between Na metal plating, which would not count towards theoretical capacity and near-Na metal plating, which would. Thus, if one is an optimist, the theoretical capacity of Na storage in amorphous carbon should be closer to 400 mAh g⁻¹, and if one is a pessimist, the capacity should be around 300 mAh g⁻¹. Capacities of 400 mAh g⁻¹ or higher are unlikely using carbon alone.

Although such an argument is not perfect, it does set the stage for future work trying to refine our initial approach at a theoretical capacity limit. Approaches could range from looking at more multatom simulations on larger graphene

sheets, with more defects, to additional work looking at clustering behavior of Na-atoms in the hard carbon structure. If anything, the search for a theoretical capacity is the most important task for computationalist involved in this sphere, as it would give experimentalists a more realistic benchmark to attain, and the opportunity to move onto other pressing issues regarding NIBs, in the event that such a benchmark has already been reached. There is no need to keep searching for the perfect carbon if we have already found it.

■ ASSOCIATED CONTENT

S Supporting Information

The Supporting Information is available free of charge on the ACS Publications website at DOI: [10.1021/acs.chemmater.8b01390](https://doi.org/10.1021/acs.chemmater.8b01390).

Schematics for justification of calculation parameters, information on unit cell size, as well as additional images of atom configurations regarding the multi-Na simulations ([PDF](#))

■ AUTHOR INFORMATION

Corresponding Author

*E-mail: alex.greaney@gmail.com.

ORCID 

Xiulei Ji: [0000-0002-4649-9594](https://orcid.org/0000-0002-4649-9594)

P. Alex Greaney: [0000-0002-4252-6022](https://orcid.org/0000-0002-4252-6022)

Notes

The authors declare no competing financial interest.

■ ACKNOWLEDGMENTS

P.A.G. and X.J. acknowledge the financial support from the National Science Foundation (NSF) of the United States, Award No. 1507391. P.A.G. also recognizes support from NSF Extreme Science and Engineering Discovery Environment (XSEDE), the UC-Riverside High-Performance Computing Cluster, and the Oregon State College of Engineering High-Performance Computing Cluster.

■ REFERENCES

- (1) Thackeray, M. M.; Wolverton, C.; Isaacs, E. D. Electrical Energy Storage for Transportation—Approaching the Limits of, and Going beyond, Lithium-Ion Batteries. *Energy Environ. Sci.* **2012**, *5*, 7854.
- (2) Pan, H.; Hu, Y.-S.; Chen, L. Room-Temperature Stationary Sodium-Ion Batteries for Large-Scale Electric Energy Storage. *Energy Environ. Sci.* **2013**, *6*, 2338.
- (3) Kim, S.-W.; Seo, D.-H.; Ma, X.; Ceder, G.; Kang, K. Electrode Materials for Rechargeable Sodium-Ion Batteries: Potential Alternatives to Current Lithium-Ion Batteries. *Adv. Energy Mater.* **2012**, *2*, 710–721.
- (4) Sawicki, M.; Shaw, L. L. Advances and Challenges of Sodium Ion Batteries as Post Lithium Ion Batteries. *RSC Adv.* **2015**, *5*, 53129–53154.
- (5) Wang, L. P.; Yu, L.; Wang, X.; Srinivasan, M.; Xu, Z. J. Recent Developments in Electrode Materials for Sodium-Ion Batteries. *J. Mater. Chem. A* **2015**, *3*, 9353–9378.
- (6) Ge, P.; Fouletier, M. Electrochemical Intercalation of Sodium in Graphite. *Solid State Ionics* **1988**, *28–30*, 1172–1175.
- (7) Doeff, M. M.; Ma, Y.; Visco, S. J.; De Jonghe, L. C. Electrochemical Insertion of Sodium into Carbon. *J. Electrochem. Soc.* **1993**, *140*, L169–L170.
- (8) Okamoto, Y. Density Functional Theory Calculations of Alkali Metal (Li, Na, and K) Graphite Intercalation Compounds. *J. Phys. Chem. C* **2014**, *118*, 16–19.

- (9) Wang, Z.; Selbach, S. M.; Grande, T. Van der Waals Density Functional Study of the Energetics of Alkali Metal Intercalation in Graphite. *RSC Adv.* **2014**, *4*, 3973–3983.
- (10) Moriwake, H.; Kuwabara, A.; Fisher, C. A. J.; Ikuhara, Y. Why Is Sodium-Intercalated Graphite Unstable? *RSC Adv.* **2017**, *7*, 36550–36554.
- (11) de la Llave, E.; Borgel, V.; Zinigrad, E.; Chesneau, F.-F.; Hartmann, P.; Sun, Y.-K.; Aurbach, D. Study of the Most Relevant Aspects Related to Hard Carbons as Anode Materials for Na-Ion Batteries, Compared with Li-Ion Systems. *Isr. J. Chem.* **2015**, *55*, 1260–1274.
- (12) Irisarri, E.; Ponrouch, A.; Palacin, M. R. Review—Hard Carbon Negative Electrode Materials for Sodium-Ion Batteries. *J. Electrochem. Soc.* **2015**, *162*, A2476–A2482.
- (13) Balogun, M.-S.; Luo, Y.; Qiu, W.; Liu, P.; Tong, Y. A Review of Carbon Materials and Their Composites with Alloy Metals for Sodium Ion Battery Anodes. *Carbon* **2016**, *98*, 162–178.
- (14) Simone, V.; Boulaineau, A.; de Geyer, A.; Rouchon, D.; Simonin, L.; Martinet, S. Hard Carbon Derived from Cellulose as Anode for Sodium Ion Batteries: Dependence of Electrochemical Properties on Structure. *J. Energy Chem.* **2016**, *25*, 761–768.
- (15) Stevens, D. A.; Dahn, J. R. High Capacity Anode Materials for Rechargeable Sodium-Ion Batteries. *J. Electrochem. Soc.* **2000**, *147*, 1271.
- (16) Stevens, D. A.; Dahn, J. R. The Mechanisms of Lithium and Sodium Insertion in Carbon Materials. *J. Electrochem. Soc.* **2001**, *148*, A803.
- (17) Ding, J.; Wang, H.; Li, Z.; Kohandehghan, A.; Cui, K.; Xu, Z.; Zahiri, B.; Tan, X.; Lotfabad, E. M.; Olsen, B. C.; Mitlin, D. Carbon Nanosheet Frameworks Derived from Peat Moss as High Performance Sodium Ion Battery Anodes. *ACS Nano* **2013**, *7*, 11004–11015.
- (18) Lotfabad, E. M.; Ding, J.; Cui, K.; Kohandehghan, A.; Kalisvaart, W. P.; Hazelton, M.; Mitlin, D. High-Density Sodium and Lithium Ion Battery Anodes from Banana Peels. *ACS Nano* **2014**, *8*, 7115–7129.
- (19) Li, Z.; Ma, L.; Surta, T. W.; Bommier, C.; Jian, Z.; Xing, Z.; Stickle, W. F.; Dolgos, M.; Amine, K.; Lu, J.; et al. High Capacity of Hard Carbon Anode in Na-Ion Batteries Unlocked by PO_x Doping. *ACS Energy Lett.* **2016**, *1*, 395–401.
- (20) Wang, X.; Han, K.; Qin, D.; Li, Q.; Wang, C.; Niu, C.; Mai, L. Polycrystalline Soft Carbon Semi-Hollow Microrods as Anode for Advanced K-Ion Full Batteries. *Nanoscale* **2017**, *9*, 18216–18222.
- (21) Ao, X.; Sun, H.; Wang, C.; Li, J.; Ruan, Y.; Li, B.; Wu, Q.-H.; Li, Y.; Jiang, J.; Yang, Y.; et al. In Situ Nitrogen-Doped Helical Mesoporous Carbonaceous Nanotubes for Superior-High Lithium Anodic Performance. *Carbon* **2018**, *130*, 599–606.
- (22) Franklin, R. E. Crystallite Growth in Graphitizing and Non-Graphitizing Carbons. *Proc. R. Soc. London, Ser. A* **1951**, *209*, 196–218.
- (23) Hasegawa, G.; Kanamori, K.; Kannari, N.; Ozaki, J.; Nakanishi, K.; Abe, T. Hard Carbon Anodes for Na-Ion Batteries: Toward a Practical Use. *ChemElectroChem* **2015**, *2*, 1917–1920.
- (24) Luo, W.; Jian, Z.; Xing, Z.; Wang, W.; Bommier, C.; Lerner, M. M.; Ji, X. Electrochemically Expandable Soft Carbon as Anodes for Na-Ion Batteries. *ACS Cent. Sci.* **2015**, *1*, 516–522.
- (25) Jian, Z.; Bommier, C.; Luo, L.; Li, Z.; Wang, W.; Wang, C.; Greaney, P. A.; Ji, X. Insights on the Mechanism of Na-Ion Storage in Soft Carbon Anode. *Chem. Mater.* **2017**, *29*, 2314–2320.
- (26) Petkov, V.; Difrancesco, R. G.; Billinge, S. J. L.; Acharya, M.; Foley, H. C. Local Structure of Nanoporous Carbons. *Philos. Mag. B* **1999**, *79*, 1519–1530.
- (27) Smith, M. A.; Foley, H. C.; Lobo, R. F. A Simple Model Describes the PDF of a Non-Graphitizing Carbon. *Carbon* **2004**, *42*, 2041–2048.
- (28) Ferrari, A. C.; Basko, D. M. Raman Spectroscopy as a Versatile Tool for Studying the Properties of Graphene. *Nat. Nanotechnol.* **2013**, *8*, 235–246.
- (29) Bommier, C.; Surta, T. W.; Dolgos, M.; Ji, X. New Mechanistic Insights on Na-Ion Storage in Nongraphitizable Carbon. *Nano Lett.* **2015**, *15*, 5888–5892.
- (30) Zhang, B.; Ghimbeu, C. M.; Laberty, C.; Vix-Guterl, C.; Tarascon, J.-M. Correlation between Microstructure and Na Storage Behavior in Hard Carbon. *Adv. Energy Mater.* **2016**, *6*, No. 1501588.
- (31) Stratford, J. M.; Allan, P. K.; Pecher, O.; Chater, P. A.; Grey, C. P. Mechanistic Insights into Sodium Storage in Hard Carbon Anodes Using Local Structure Probes. *Chem. Commun.* **2016**, *52*, 12430–12433.
- (32) Datta, D.; Li, J.; Shenoy, V. B. Defective Graphene as a High-Capacity Anode Material for Na- and Ca-Ion Batteries. *ACS Appl. Mater. Interfaces* **2014**, *6*, 1788–1795.
- (33) Shen, H.; Rao, D.; Xi, X.; Liu, Y.; Shen, X. N-Substituted Defective Graphene Sheets: Promising Electrode Materials for Na-Ion Batteries. *RSC Adv.* **2015**, *5*, 17042–17048.
- (34) Legrain, F.; Kotsis, K.; Manzhos, S. Amorphous Carbon a Promising Material for Sodium Ion Battery Anodes: A First Principles Study. **2015**, arXiv:1502.00833. arXiv.org e-Print archive. <https://arxiv.org/abs/1502.00833>.
- (35) Legrain, F.; Malyi, O. I.; Manzhos, S. Comparative Computational Study of the Energetics of Li, Na, and Mg Storage in Amorphous and Crystalline Silicon. *Comput. Mater. Sci.* **2014**, *94*, 214–217.
- (36) Tsai, P.; Chung, S.-C.; Lin, S.; Yamada, A. Ab Initio Study of Sodium Intercalation into Disordered Carbon. *J. Mater. Chem. A* **2015**, *3*, 9763–9768.
- (37) Malyi, O. I.; Sopiha, K.; Kulish, V. V.; Tan, T. L.; Manzhos, S.; Persson, C. A Computational Study of Na Behavior on Graphene. *Appl. Surf. Sci.* **2015**, *333*, 235–243.
- (38) Yang, S.; Li, S.; Tang, S.; Dong, W.; Sun, W.; Shen, D.; Wang, M. Sodium Adsorption and Intercalation in Bilayer Graphene from Density Functional Theory Calculations. *Theor. Chem. Acc.* **2016**, *135*, 164.
- (39) Yang, S.; Li, S.; Tang, S.; Shen, D.; Dong, W.; Sun, W. Adsorption, Intercalation and Diffusion of Na on Defective Bilayer Graphene: A Computational Study. *Surf. Sci.* **2017**, *658*, 31–37.
- (40) Wang, Z.; Ratvik, A. P.; Grande, T.; Selbach, S. M. Diffusion of Alkali Metals in the First Stage Graphite Intercalation Compounds by VdW-DFT Calculations. *RSC Adv.* **2015**, *5*, 15985–15992.
- (41) Dobrota, A. S.; Pašti, I. A.; Mentus, S. V.; Johansson, B.; Skorodumova, N. V. Functionalized Graphene for Sodium Battery Applications: The DFT Insights. *Electrochim. Acta* **2017**, *250*, 185–195.
- (42) Ladha, D. G. A Review on Density Functional Theory-Based Study on Two-Dimensional Materials Used in Batteries. *Mater. Today Chem.* **2019**, *11*, 94–111.
- (43) Kresse, G.; Hafner, J. Ab Initio Molecular Dynamics for Liquid Metals. *Phys. Rev. B* **1993**, *47*, 558.
- (44) Kresse, G.; Hafner, J. Ab Initio Molecular-Dynamics Simulation of the Liquid-Metal–Amorphous-Semiconductor Transition in Germanium. *Phys. Rev. B* **1994**, *49*, 14251.
- (45) Kresse, G.; Furthmüller, J. Efficient Iterative Schemes for Ab Initio Total-Energy Calculations Using a Plane-Wave Basis Set. *Phys. Rev. B* **1996**, *54*, 11169.
- (46) Blöchl, P. E. Projector Augmented-Wave Method. *Phys. Rev. B* **1994**, *50*, 17953.
- (47) Kresse, G.; Joubert, D. From Ultrasoft Pseudopotentials to the Projector Augmented-Wave Method. *Phys. Rev. B* **1999**, *59*, 1758.
- (48) Perdew, J. P.; Burke, K.; Ernzerhof, M. Generalized Gradient Approximation Made Simple. *Phys. Rev. Lett.* **1996**, *77*, 3865.
- (49) Grimme, S.; Antony, J.; Ehrlich, S.; Krieg, H. A Consistent and Accurate Ab Initio Parametrization of Density Functional Dispersion Correction (DFT-D) for the 94 Elements H-Pu. *J. Chem. Phys.* **2010**, *132*, No. 154104.
- (50) Grimme, S.; Ehrlich, S.; Goerigk, L. Effect of the Damping Function in Dispersion Corrected Density Functional Theory. *J. Comput. Chem.* **2011**, *32*, 1456–1465.

- (51) Monkhorst, H. J.; Pack, J. D. Special Points for Brillouin-Zone Integrations. *Phys. Rev. B* **1976**, *13*, 5188.
- (52) Legrain, F.; Sottmann, J.; Kotsis, K.; Gorantla, S.; Sartori, S.; Manzhos, S. Amorphous (Glassy) Carbon, a Promising Material for Sodium Ion Battery Anodes: A Combined First-Principles and Experimental Study. *J. Phys. Chem. C* **2015**, *119*, 13496–13501.
- (53) Xiao, B.; Li, Y.; Yu, X.; Cheng, J. Penta-Graphene: A Promising Anode Material As the Li/Na-Ion Battery with Both Extremely High Theoretical Capacity and Fast Charge/Discharge Rate. *ACS Appl. Mater. Interfaces* **2016**, *8*, 35342–35352.
- (54) Sun, X.; Wang, Z.; Fu, Y. Q. Adsorption and Diffusion of Sodium on Graphene with Grain Boundaries. *Carbon* **2017**, *116*, 415–421.
- (55) Lotfabad, E. M.; Kalisvaart, P.; Kohandehghan, A.; Karpuzov, D.; Mitlin, D. Origin of Non-SEI Related Coulombic Efficiency Loss in Carbons Tested against Na and Li. *J. Mater. Chem. A* **2014**, *2*, 19685–19695.
- (56) Ding, J.; Zhou, H.; Zhang, H.; Stephenson, T.; Li, Z.; Karpuzov, D.; Mitlin, D. Exceptional Energy and New Insight with a Sodium–Selenium Battery Based on a Carbon Nanosheet Cathode and a Pseudographite Anode. *Energy Environ. Sci.* **2017**, *10*, 153–165.
- (57) Nobuhara, K.; Nakayama, H.; Nose, M.; Nakanishi, S.; Iba, H. First-Principles Study of Alkali Metal-Graphite Intercalation Compounds. *J. Power Sources* **2013**, *243*, 585–587.
- (58) Liu, Y.; Merinov, B. V.; Goddard, W. A. Origin of Low Sodium Capacity in Graphite and Generally Weak Substrate Binding of Na and Mg among Alkali and Alkaline Earth Metals. *Proc. Natl. Acad. Sci. U.S.A.* **2016**, *113*, 3735–3739.
- (59) Koh, Y. W.; Manzhos, S. Curvature Drastically Changes Diffusion Properties of Li and Na on Graphene. *MRS Commun.* **2013**, *3*, 171–175.
- (60) Safran, S.; Hamann, D. Long-Range Elastic Interactions and Staging in Graphite Intercalation Compounds. *Phys. Rev. Lett.* **1979**, *42* (21), 1410.
- (61) Jian, Z.; Bommier, C.; Luo, L.; Li, Z.; Wang, W.; Wang, C.; Greaney, P. A.; Ji, X. Insights on the Mechanism of Na-Ion Storage in Soft Carbon Anode. *Chem. Mater.* **2017**, 2314.
- (62) Fan, X.; Zheng, W.; Kuo, J.-L.; Singh, D. J. Adsorption of Single Li and the Formation of Small Li Clusters on Graphene for the Anode of Lithium-Ion Batteries. *ACS Appl. Mater. Interfaces* **2013**, *5*, 7793–7797.
- (63) Liang, Z.; Fan, X.; Zheng, W.; Singh, D. J. Adsorption and Formation of Small Na Clusters on Pristine and Double-Vacancy Graphene for Anodes of Na-Ion Batteries. *ACS Appl. Mater. Interfaces* **2017**, *9*, 17076–17084.
- (64) Niaezi, A. H. F.; Hussain, T.; Hankel, M.; Searles, D. J. Hydrogenated Defective Graphene as an Anode Material for Sodium and Calcium Ion Batteries: A Density Functional Theory Study. *Carbon* **2018**, *136*, 73–84.